DESY 09-081
June 2009

Anatomy of the pQCD Approach to the Baryonic Decays $\Lambda_b \to p\pi,\ pK$

Cai-Dian Lü, Yu-Ming Wang, Hao Zou
Institute of High Energy Physics and
Theoretical Physics Center for Science Facilities,
CAS, P.O. Box 918(4), 100049,
People's Republic of China

Ahmed Ali[a] and Gustav Kramer[b]
[a] *Deutsches Elektronen-Synchrotron DESY, 22607 Hamburg, Germany*
[b] *II. Institut für Theoretische Physik, Universität Hamburg, 22761 Hamburg, Germany*

(Dated: August 3, 2009)

We calculate the CP-averaged branching ratios and CP-violating asymmetries for the two-body charmless hadronic decays $\Lambda_b \to p\pi,\ pK$ in the perturbative QCD (pQCD) approach to lowest order in α_s. The baryon distribution amplitudes involved in the factorization formulae are considered to the leading twist accuracy and the distribution amplitudes of the proton are expanded to the next-to-leading conformal spin (i.e., "P" -waves), the moments of which are determined from QCD sum rules. Our work shows that the contributions from the factorizable diagrams in $\Lambda_b \to p\pi,\ pK$ decays are much smaller compared to the non-factorizable diagrams in the conventional pQCD approach. We argue that this reflects the estimates of the $\Lambda_b \to p$ transition form factors in the k_T factorization approach, which are found typically an order of magnitude smaller than those estimated in the light-cone sum rules and in the non-relativistic quark model. As an alternative, we adopt a hybrid pQCD approach, in which we compute the factorizable contributions with the $\Lambda_b \to p$ form factors taken from the light cone QCD sum rules. The non-factorizable diagrams are evaluated utilizing the conventional pQCD formalism which is free from the endpoint singularities. The predictions worked out here are confronted with the recently available data from the CDF collaboration on the branching ratios and the direct CP asymmetries for the decays $\Lambda_b \to p\pi$, and $\Lambda_b \to pK$. The asymmetry parameter α relevant for the anisotropic angular distribution of the emitted proton in the polarized Λ_b baryon decays is also calculated for the two decay modes.

PACS numbers: 14.20.Mr, 12.38.Bx, 12.39.St, 13.30.Eg

I. INTRODUCTION

The motivation to investigate b quark decays is attributed to their sensitivity to the quark flavor structure, which leads to an extremely rich phenomenology, studied mostly in the context of B-meson decays. However, heavy baryons containing a b-quark have been observed at the Tevatron and they will be even more copiously produced at the large hadron collider (LHC). Their weak decays may provide important clues on the flavor-changing currents beyond the standard model (SM) in a complementary fashion to the B meson decays. A particular advantage of the bottom baryons over B-mesons is their spin, which provides a unique way to analyze the helicity structure of the effective Hamiltonian for the weak transition in the SM and beyond. Also, such baryon decays are flavor self-tagging processes which should make their experimental reconstructions easier.

Theoretical analysis of non-leptonic decays are based on factorization theorems, which are the fundamental tools of the QCD perturbation theory enabling the separation of physics at different energy scales. The theoretical basis of the factorization theorem is a generalization of the Euclidean operator product expansion to the time-like domain. The proof of the factorization theorem has been worked out using the perturbative QCD approach based on the analysis of Feynman diagrams in the so called Collins-Soper-Sterman (CSS) formalism [1, 2, 3]. Equally importantly, the large mass of the heavy quark makes the formidable strong interactions effects controllable and they can be studied systematically using methods based on heavy quark expansion.

The basic formula for the calculation of the branching ratios for the decays of the Λ_b baryon into two light hadrons is based on an operator realization of the diagrammatic analysis which can be described most easily for the calculation of the hadronic matrix element of B mesons decays into two light hadrons h_1 and h_2. With the insertion of a set of the weak interaction operator O_i between the initial B meson and the final decay products h_1 and h_2, the decay matrix element is obtained from the following formula [4]

$$\langle h_1 h_2|\mathcal{O}_i|B\rangle = \Phi_{h_2}(u) \otimes \Big(T^I(u) F^{Bh_1}(0) + C^{II}(\tau,u) \otimes \Xi^{Bh_1}(\tau,0)\Big) \tag{1}$$

involving the QCD form factor $F^{Bh_1}(0)$ and an unknown, non-local form factor $\Xi^{Bh_1}(\tau,0)$ at the leading power in the Λ/m_b expansion. Different treatments of the various parts in the factorization formula (1) have led to three popular theoretical approaches to study the dynamics of non-leptonic two-body B meson decays, which are known as the perturbative QCD (pQCD) [5], QCD factorization (QCDF) [6] and SCET approaches [7, 8, 9]. The function $\Xi^{Bh_1}(\tau,0)$ is supposed to be dominated by perturbative hard-collinear interactions, and can be further factorized into light-cone

distribution amplitudes $\Phi_B(\omega)$, $\Phi_{h_1}(v)$ and a jet function $J(\tau;\omega,v)$

$$\Xi^{Bh_1}(\tau,0) = J(\tau;\omega,v) \otimes \Phi_B(\omega) \otimes \Phi_{h_1}(v), \tag{2}$$

when the hard-collinear scale $\sqrt{m_b \Lambda_{QCD}}$ is integrated out [10].

In contrast to these two latter approaches based on the collinear factorization theorem, the pQCD approach, which is developed in the framework of k_T factorization, is free of the singularities from the end-point region of the parton momentum fractions. The pQCD approach has been widely applied for the calculation of the non-leptonic two-body B decays and it has proved itself to be successful in the description of exclusive processes with typical momentum-transfer of a few GeV. A hallmark of this approach is that the form factor $F^{Bh_1}(0)$ is assumed to be dominated by short-distance contributions and it is therefore calculable in the perturbative theory. Soft contributions, though playing a role, are less important because of the suppression from the Sudakov mechanism embedded in the k_T and threshold resummations [11]. Current applications of the k_T factorization theorem to exclusive processes are restricted to the leading order (LO) in the strong coupling constant α_s. In this, the infrared divergences involved in the radiative corrections to the weak transition vertex are absorbed in the hadronic distribution amplitudes in a gauge invariant manner. The factorizable, non-factorizable and power-suppressed annihilation contributions are calculable in this framework free of the end-point singularities.

In the case of non-leptonic two-body B decays, the decay matrix elements, in most cases, are dominated by the factorizable term, i.e. the first term on the right-hand side of Eq. (1), whereas the second term, the non-factorizable one, produces a perturbative correction. Since the first term proportional to the form factor $F^{Bh_1}(0)$ is in pQCD very similar to the other approaches, where the form factors are input, the pQCD approach gives in most cases similar results for the non-leptonic B decays as the other two approaches mentioned above, though there are differences in detail.

In the application of pQCD to two-body non-leptonic heavy baryon decays, we do not expect a similar pattern as in the non-leptonic B meson decays on general grounds. In particular, in the analysis of the hadronic decays of baryons, a large number of Feynman diagrams contribute to the hard amplitudes even in the lowest-order. Taking the $\Lambda_b \to p\pi$ decay as an example, some 200 Feynman diagrams need to be calculated as can be seen in section III. These diagrams involve the exchange of two gluons, involving topologies where both gluons are attached to one of the light quarks emerging from the weak interaction vertex. As some of these diagrams build up the transition form factor, they receive contributions in α_s^2, yielding small values for them. Another challenge for the baryonic transition is that the light-cone distribution amplitudes (LCDAs) of

the baryons are less known in the literature. LCDAs are fundamental non-perturbative input to regularize the infrared divergence appearing in the radiative corrections in the factorization formalism of the pQCD approach. In view of this, applications of the pQCD approach to non-leptonic two-body b-baryon decays are not worked out to a satisfactory level, and hence this area is essentially an uncharted territory.

A first attempt to apply the pQCD approach to the baryonic transitions was made in [12], where the proton Dirac form factor is calculated taking into account the Sudakov suppression resulting from the resummation of the large double logarithms involved in the radiative corrections. Subsequently, the proton form factor was recalculated in [13] by refining the choice of the evolution scale of the proton wave functions and the infrared cutoffs for the Sudakov resummation, which lead to predictions for the Dirac form factors which are consistent with the experimental data. Following Refs. [12, 13], the semileptonic charmless decays $\Lambda_b \to p l\bar{\nu}$ [14], the semileptonic charming decay $\Lambda_b \to \Lambda_c l\bar{\nu}$ [15, 16], the radiative decay $\Lambda_b \to \Lambda\gamma$ [17], and the nonleptonic charming decay $\Lambda_b \to \Lambda J/\psi$ [18] have been investigated in the framework of the k_T factorization scheme. However, a study of the charmless hadronic decays $\Lambda_b \to h_1 h_2$, which has been undertaken in the generalized factorization approach [19, 20], to the best of our knowledge, is still lacking in pQCD. Our aim is to fill in this gap and provide further tests of the k_T factorization formalism to gain insight on the QCD dynamics of these decays. In doing this, we have included the current information on the CKM matrix elements, updated some input hadronic parameters, such as the distribution amplitudes of the proton, which are systematically studied in [21] making use of the conformal symmetry of the QCD Lagrangian, and have used data to fix some other input quantities. We find that the non-factorizable contributions to the hard amplitudes overwhelm the ones from the factorizable diagrams in the baryonic decays $\Lambda_b \to p\pi,\ pK$. This feature of the b-baryonic decays is at variance with what is found in the naive factorization approximation and in the corresponding two-body B meson decays. Large non-factorizable effects existing in the charmed baryon decays have been pointed out in the literature [22], where it is observed that the non-factorizable diagrams escaping from the helicity and color suppression can be comparable to and sometimes even dominate over the factorizable contributions.

The layout of the paper is as follows: In section II, we briefly review the pQCD approach and give the essential input quantities that enter this approach, including the operator basis used subsequently and the LCDAs for the pseudoscalar mesons, the proton as well as the Λ_b baryon. Input values of the various mesonic decay constants and the baryonic wave function at the origin in configuration space are also collected there. Section III contains the calculation of the $\Lambda_b \to p\pi,\ pK$

decays, making explicit the contributions from the external W emission diagrams T, the internal W emission diagrams C, the W exchange diagram E, the bow-tie contraction diagrams B and the penguin diagrams P, as shown in Fig. 3. Details of the calculations are relegated to the two Appendices (Appendix A, where the Fourier integration to derive the hard amplitudes in the impact parameter (or b) space are displayed, and Appendix B, where the factorization formulae for the Feynman diagrams corresponding to various toplogies are given). The decay amplitudes called f_1 and f_2, defined in Eq. (44), resulting from the diagrams with different topologies evaluated in the conventional pQCD approach are given numerically in Table III. We find that the T diagrams dominate the $\Lambda_b \to p\pi,\ pK$ decays, as expected. Numerical values of the factorizable and non-factorizable contributions from the T diagram amplitudes $f_i(\Lambda_b \to p\pi,\ pK); i = 1, 2$, in the conventional pQCD approach are given in Table IV. From the entries in this table we observe that the factorizable amplitudes in these decays are essentially two orders of magnitude smaller than the corresponding non-factorizable amplitudes. The form factor g_1 responsible for the $\Lambda_b \to p$ transition evaluated in various theoretical approaches are collected in Table V, and we find that g_1 calculated in the pQCD approach is typically an order of magnitude smaller than in other approaches [19, 23], where the form factors are dominated by soft dynamics. Subsequently, we employ a hybrid prescription to deal with the hadronic $\Lambda_b \to p\pi,\ pK$ decays. In this approach, the factorizable contributions are parametrized in the naive factorization approximation, and the variation of the renormalization scale is assumed to reflect the effect of the vertex corrections. The non-factorizable diagrams are evaluated, as in the conventional pQCD approach, in the framework of the k_T factorization. Following this procedure and utilizing the from factors calculated in the light-cone sum rules (LCSR), we reanalyze these two channels and give the numerical results for the amplitudes $f_i(\Lambda_b \to p\pi,\ pK); i = 1, 2$, for the factorizable and non-factorizable contributions from the hybrid scheme in Table VII. We note that the factorizable contributions are much larger in the hybrid scheme and they constitute a good fraction of the corresponding non-factoriazable amplitudes. Numerical results for the charge-conjugated averages of the decay branching ratios, direct CP-asymmetries and polarization asymmetry parameter α are tabulated in Table VIII. A comparison of our predictions with the available experimental data [24] are also included in this table. Section IV contains our conclusion and an outlook.

II. CONVENTIONS, INPUTS AND SOME FORMULAE IN PQCD

A. Effective Hamiltonian

We specify the weak effective Hamiltonian [25]:

$$\mathcal{H}_{eff} = \frac{G_F}{\sqrt{2}}\Big\{V_{ub}V_{uq}^*\Big[C_1(\mu)Q_1^u(\mu)+C_2(\mu)Q_2^u(\mu)\Big]-V_{tb}V_{tq}^*\Big[\sum_{i=3}^{10}C_i(\mu)Q_i(\mu)\Big]\Big\}+\text{h.c.}, \tag{3}$$

where $q=d,s$. The functions Q_i $(i=1,...,10)$ are the local four-quark operators:

- current–current (tree) operators

$$Q_1^u=(\bar{u}_\alpha b_\beta)_{V-A}(\bar{q}_\beta u_\alpha)_{V-A}, \qquad Q_2^u=(\bar{u}_\alpha b_\alpha)_{V-A}(\bar{q}_\beta u_\beta)_{V-A}, \tag{4}$$

- QCD penguin operators

$$Q_3=(\bar{q}_\alpha b_\alpha)_{V-A}\sum_{q'}(\bar{q}'_\beta q'_\beta)_{V-A}, \qquad Q_4=(\bar{q}_\beta b_\alpha)_{V-A}\sum_{q'}(\bar{q}'_\alpha q'_\beta)_{V-A}, \tag{5}$$

$$Q_5=(\bar{q}_\alpha b_\alpha)_{V-A}\sum_{q'}(\bar{q}'_\beta q'_\beta)_{V+A}, \qquad Q_6=(\bar{q}_\beta b_\alpha)_{V-A}\sum_{q'}(\bar{q}'_\alpha q'_\beta)_{V+A}, \tag{6}$$

- electro-weak penguin operators

$$Q_7=\frac{3}{2}(\bar{q}_\alpha b_\alpha)_{V-A}\sum_{q'}e_{q'}(\bar{q}'_\beta q'_\beta)_{V+A}, \qquad Q_8=\frac{3}{2}(\bar{q}_\beta b_\alpha)_{V-A}\sum_{q'}e_{q'}(\bar{q}'_\alpha q'_\beta)_{V+A}, \tag{7}$$

$$Q_9=\frac{3}{2}(\bar{q}_\alpha b_\alpha)_{V-A}\sum_{q'}e_{q'}(\bar{q}'_\beta q'_\beta)_{V-A}, \qquad Q_{10}=\frac{3}{2}(\bar{q}_\beta b_\alpha)_{V-A}\sum_{q'}e_{q'}(\bar{q}'_\alpha q'_\beta)_{V-A}, \tag{8}$$

where α and β are the color indices and q' are the active quarks at the scale m_b, i.e. $q'=(u,d,s,c,b)$. The left handed current is defined as $(\bar{q}'_\alpha q'_\beta)_{V-A}=\bar{q}'_\alpha\gamma_\nu(1-\gamma_5)q'_\beta$ and the right handed current as $(\bar{q}'_\alpha q'_\beta)_{V+A}=\bar{q}'_\alpha\gamma_\nu(1+\gamma_5)q'_\beta$. For later applications it will be convenient to use the following combinations of the Wilson coefficients Q_i [26]:

$$\begin{aligned} &a_1=C_2+C_1/3,\ a_3=C_3+C_4/3,\ a_5=C_5+C_6/3,\ a_7=C_7+C_8/3,\ a_9=C_9+C_{10}/3,\\ &a_2=C_1+C_2/3,\ a_4=C_4+C_3/3,\ a_6=C_6+C_5/3,\ a_8=C_8+C_7/3,\ a_{10}=C_{10}+C_9/3, \end{aligned} \tag{9}$$

where the scale dependence for the Wilson coefficients has been suppressed here. For convenience, we have given the combinations a_i of the Wilson coefficients at three different values of the energy scale in Table. I.

TABLE I: Numerical values of the effective Wilson coefficients defined in the text at three different scales μ, where m_b is taken as 4.8 GeV.

μ (GeV)	$0.5m_b$	m_b	$1.5m_b$
a_1	1.06	1.03	1.02
$a_2(\times 10^{-2})$	0.40	10.3	14.8
$a_3(\times 10^{-3})$	6.41	3.60	2.63
$a_4(\times 10^{-3})$	-32.6	-22.8	-18.3
$a_5(\times 10^{-3})$	-5.87	-2.29	-1.20
$a_6(\times 10^{-3})$	-48.2	-29.8	-22.5
$a_7(\times 10^{-4})$	12.6	12.2	12.0
$a_8(\times 10^{-4})$	9.79	7.57	6.69
$a_9(\times 10^{-4})$	-84.5	-82.2	-81.4
$a_{10}(\times 10^{-4})$	-0.32	-8.20	-11.9

B. Kinematics

The kinematic variables of the initial and final hadrons can be defined as follows. The Λ_b baryon is assumed to be at rest, and the proton recoils in the minus z direction. p, p' and $q = p - p'$ denote the momentum of the Λ_b baryon, the proton and the light meson, respectively. The momenta of their valence quarks are parametrized as

$$
\begin{aligned}
&p = (p^+, p^-, \mathbf{0}) = \frac{M_{\Lambda_b}}{\sqrt{2}}(1, 1, \mathbf{0}) \,, \\
&k_1 = (x_1 p^+, p^-, \mathbf{k}_{1T}) \,, \quad k_2 = (x_2 p^+, 0, \mathbf{k}_{2T}) \,, \quad k_3 = (x_3 p^+, 0, \mathbf{k}_{3T}) \,, \\
&p' = (0, p'^-, \mathbf{0}) = (0, p^-, \mathbf{0}) \,, \\
&k_1' = (0, x_1' p'^-, \mathbf{k}'_{1T}) \,, \quad k_2' = (0, x_2' p'^-, \mathbf{k}'_{2T}) \,, \quad k_3' = (0, x_3' p'^-, \mathbf{k}'_{3T}) \,, \\
&q = (q^+, 0, \mathbf{0}) = (p^+, 0, \mathbf{0}) \,, \\
&q_1 = (y q^+, 0, \mathbf{q}_T) \,, \quad q_2 = ((1-y) q^+, 0, -\mathbf{q}_T) \,,
\end{aligned}
\tag{10}
$$

where k_1 (k_1') is the b (u) quark momentum, x_i (x_i') are their longitudinal momentum fractions, and $\mathbf{k}_{iT}^{(\prime)}$ are the corresponding transverse momenta, satisfying $\sum_l \mathbf{k}_{lT}^{(\prime)} = 0$. y is the longitudinal momentum fraction carried by the quark in the emitted light meson and $\mathbf{q}_T$ is its transverse momentum. The kinematics of the non-leptonic two body decays of Λ_b is described in Fig. 1.

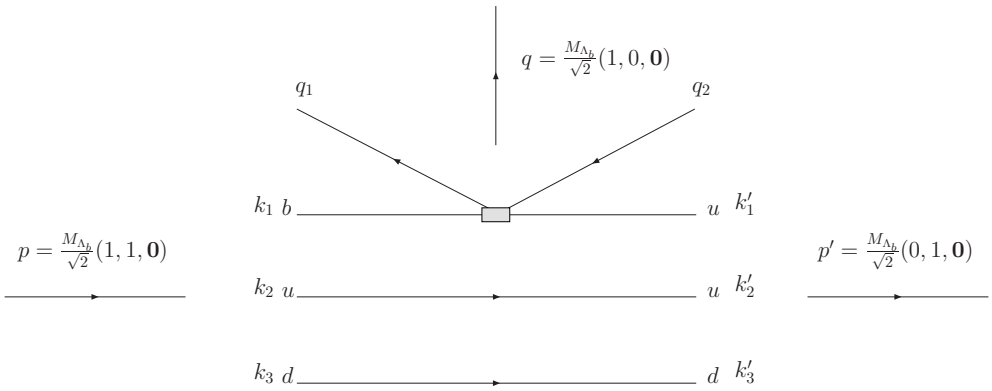

FIG. 1: Kinematics of the non-leptonic two-body decays of Λ_b in the pQCD approach.

C. Distribution amplitudes of pseudoscalar mesons

The light-cone distribution amplitudes for the pseudoscalar meson are given by [27, 28]

$$\begin{aligned}\langle P(P)|\bar{q}_{2\beta}(z)q_{1\alpha}(0)|0\rangle &= -\frac{i}{\sqrt{6}}\int_0^1 dx e^{ixP\cdot z}\left[\gamma_5 \not{P}\phi^A(x) + m_0\gamma_5\phi^P(x) - m_0\sigma^{\mu\nu}\gamma_5 P_\mu z_\nu\frac{\phi^\sigma(x)}{6}\right]_{\alpha\beta}\\ &= -\frac{i}{\sqrt{6}}\int_0^1 dx e^{ixP\cdot z}\left[\gamma_5 \not{P}\phi^A(x) + \gamma_5 m_0\phi^P(x) + m_0\gamma_5(\not{n}\not{v}-1)\phi^T(x)\right]_{\alpha\beta},\end{aligned} \tag{11}$$

where

$$\phi_\pi^A(x) = \frac{3f_\pi}{\sqrt{6}}x(1-x)[1+0.44C_2^{3/2}(t)], \tag{12}$$

$$\phi_\pi^P(x) = \frac{f_\pi}{2\sqrt{6}}[1+0.43C_2^{1/2}(t)], \tag{13}$$

$$\phi_\pi^T(x) = -\frac{f_\pi}{2\sqrt{6}}[C_1^{1/2}(t)+0.55C_3^{1/2}(t)], \tag{14}$$

$$\phi_K^A(x) = \frac{3f_K}{\sqrt{6}}x(1-x)[1+0.17C_1^{3/2}(t)+0.115C_2^{3/2}(t)], \tag{15}$$

$$\phi_K^P(x) = \frac{f_K}{2\sqrt{6}}[1+0.24C_2^{1/2}(t)], \tag{16}$$

$$\phi_K^T(x) = -\frac{f_K}{2\sqrt{6}}[C_1^{1/2}(t)+0.35C_3^{1/2}(t)], \tag{17}$$

and the Gegenbauer polynomials are defined as:

$$\begin{aligned} &C_1^{1/2}(t) = t, && C_1^{3/2}(t) = 3t\\ &C_2^{1/2}(t) = \tfrac{1}{2}(3t^2-1), && C_2^{3/2}(t) = \tfrac{3}{2}(5t^2-1),\\ &C_3^{1/2}(t) = \tfrac{1}{2}t(5t^2-3), &&\\ &C_4^{1/2}(t) = \tfrac{1}{8}(35t^4-30t^2+3), && C_4^{3/2}(t) = \tfrac{15}{8}(21t^4-14t^2+1),\end{aligned} \tag{18}$$

and $t = 2x - 1$. The decay constants of these mesons are fixed as $f_\pi = 130$ MeV and $f_K = 160$ MeV in our numerical calculations.

D. Distribution amplitudes of baryons

1. *Distribution amplitudes of the Λ_b baryon*

The Lorentz structure of the Λ_b baryon wave function Y_{Λ_b} can be simplified using the Bargmann-Wigner equation [29] in the heavy quark limit, where the spin and orbital degrees of freedom of the light quark system are decoupled. In the transverse momentum space, the wave function of the Λ_b baryon is defined as [30, 31]

$$\begin{aligned}(Y_{\Lambda_b})_{\alpha\beta\gamma}(k_i,\mu) &= \frac{1}{2\sqrt{2}N_c}\int\prod_{l=2}^{3}\frac{dw_l^- d\mathbf{w}_l}{(2\pi)^3}e^{ik_l\cdot w_l}\epsilon^{ijk}\langle 0|T[b^i_\alpha(0)u^j_\beta(w_2)d^k_\gamma(w_3)]|\Lambda_b(p)\rangle\ ,\\ &= \frac{f_{\Lambda_b}}{8\sqrt{2}N_c}[(\not{p}+M_{\Lambda_b})\gamma_5 C]_{\beta\gamma}[\Lambda_b(p)]_\alpha\psi(k_i,\mu)\ ,\end{aligned} \tag{19}$$

where b, u, and d are the quark fields, i, j, and k are the color indices, α, β and γ are the spinor indices, C is the charge conjugation matrix, $\Lambda_b(p)$ is the Λ_b baryon spinor. The normalization constant corresponds to the value of the wave function at the origin in the configuration space. The numerical value $f_{\Lambda_b} = 4.28^{+0.75}_{-0.64}\times 10^{-3}$ GeV^2 used by us is determined from the experimental data on the semileptonic decay $\Lambda_b \to \Lambda_c l\bar{\nu}_l$ [32]. The quoted value (within the $\pm 1\sigma$ range) is also in agreement with the ones estimated in the QCD sum rule (QCDSR) approach [33, 34].

The phenomenological model for the distribution amplitude of the Λ_b baryon employed in this work is borrowed from [35]

$$\psi(x_1,x_2,x_3) = Nx_1x_2x_3\exp\Big[-\frac{M^2_{\Lambda_b}}{2\beta^2x_1}-\frac{m_l^2}{2\beta^2x_2}-\frac{m_l^2}{2\beta^2x_3}\Big] \tag{20}$$

with the shape parameter $\beta = 1.0 \pm 0.2$ GeV and the mass of the light degrees of freedom in the Λ_b baryon being $m_l = 0.3$ GeV. The normalization

$$\int [dx]\psi(x_1,x_2,x_3) = 1\ , \tag{21}$$

leads to the constant $N = 6.67\times 10^{12}$. We point out that the complete set of three-quark distributions amplitudes of the Λ_b baryon has been investigated in Ref. [36] in the heavy quark limit and the renormalization-group equation governing the scale-dependence of the leading twist distribution amplitude is also derived there. It is shown that the evolution equation for the leading twist distribution amplitude includes a piece associated with the Lange-Neubert kernel [37] which

generates a radiative tail extending to high energies, and a piece relevant to the Brodsky-Lepage kernel [38], which redistributes the momentum within the spectator diquark system. It is sufficient to limit the accuracy of the current pQCD analysis to the leading twist approximation due to the still large errors of the experimental data.

The model for the twist-2 distribution amplitude for the Λ_b baryon proposed in [36] is:

$$\psi^{\rm QCD}(\omega,u) = \omega^2 u(1-u)\Big[\frac{1}{\epsilon_0^4}e^{-\frac{\omega}{\epsilon_0}} + a_2 C_2^{3/2}(2u-1)\frac{1}{\epsilon_1^4}e^{-\frac{\omega}{\epsilon_1}}\Big] \tag{22}$$

with $\epsilon_0 = 200^{+130}_{-60}$MeV, $\epsilon_1 = 650^{+650}_{-300}$MeV and $a_2 = 0.333^{+0.250}_{-0.333}$. In the above representation, ω is the total energy carried by the light quarks in the rest frame of Λ_b baryon and the dimensionless parameter u describes the momentum fraction carried by the u quark in the diquark system. The normalization of $\psi^{\rm QCD}(\omega,u)$ is

$$\int_0^\infty \omega d\omega \int_0^1 du \psi^{\rm QCD}(\omega,u) = 1. \tag{23}$$

For comparison, we translate Eq. (20) in terms of the variables ω and u of Ref. [36]:

$$\begin{aligned}\psi^{\rm CQM}(\omega,u) \;=\; & \frac{1}{M_{\Lambda_b}^4} N\omega^2 u(1-u)\Big[1-\frac{u\omega}{M_{\Lambda_b}}-\frac{(1-u)\omega}{M_{\Lambda_b}}\Big] \\ & \times\exp\Big[-\frac{M_{\Lambda_b}^2}{2\beta^2(1-\frac{u\omega}{M_{\Lambda_b}}-\frac{(1-u)\omega}{M_{\Lambda_b}})}-\frac{m_l^2}{2\beta^2\frac{u\omega}{M_{\Lambda_b}}}-\frac{m_l^2}{2\beta^2\frac{(1-u)\omega}{M_{\Lambda_b}}}\Big].\end{aligned} \tag{24}$$

The shapes of the LCDAs $\psi^{\rm QCD}(\omega,u)$ and $\psi^{\rm CQM}(\omega,u)$, given in Eqs. (22) and (24), respectively, are shown in Fig. 2, and the various curves show the dependence on the input parameters of the models. The variations of a_2 in $\psi^{\rm QCD}(\omega,u)$ does not play a significant role in the behavior of $\psi^{\rm QCD}(\omega,u)$, since the second moment is suppressed by ϵ_0/ϵ_1, and so we have fixed $a_2 = 0.333$. At this stage, it is difficult to select one or the other of these LCDAs. The harder spectrum of $\psi^{CQM}(\omega,u)$ in ω (the sum of the energy of the two light quarks in the rest frame of the Λ_b-baryon) also reflects in the inverse moments, which are more important for the dynamics. Following Ref. [36], we define the two inverse moments involving negative powers of the variables ω and u, the fractional quark momentum

$$\langle(\omega u)^{-1}(\Lambda_{UV})\rangle \equiv \int_0^{\Lambda_{UV}} d\omega \int_0^1 \frac{du}{u}\psi^{QCD/CQM}(\omega,u), \qquad \langle\omega^{-1}(\Lambda_{UV})\rangle \equiv \int_0^{\Lambda_{UV}} d\omega \int_0^1 du\psi^{QCD/CQM}(\omega,u), \tag{25}$$

where an additional energy cut $\omega < \Lambda_{UV}$ is introduced to guarantee that the moments are finite in the presence of a radiative tail. The values of $\langle(\omega u)^{-1}\rangle$ and $\langle\omega^{-1}\rangle$ for $\Lambda_{UV} = 2.5$ GeV and $\mu = 1$ GeV are summarized in Table II. We note from this table that the moments of the two

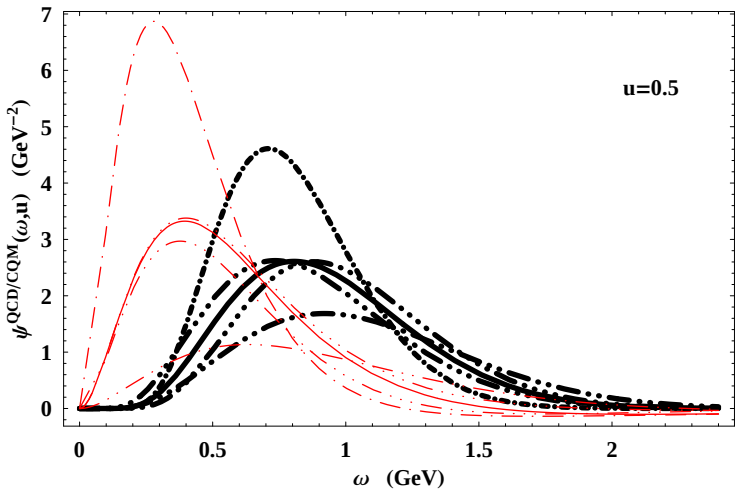

FIG. 2: The functions $\psi^{QCD}(\omega,u)$ and $\psi^{CQM}(\omega,u)$ plotted against ω for the fixed value $u=0.5$. The solid, dashed-dotted, dashed-double-dotted, dashed-triple-dotted, and dashed-quartic-dotted curves, peaking typically around $\omega=0.8$ GeV, describe the distribution amplitude $\psi^{CQM}(\omega,u)$ with the values of the parameters ($\beta=1.0$ GeV, $m_l=0.3$ GeV), ($\beta=0.8$ GeV, $m_l=0.30$ GeV), ($\beta=1.2$ GeV, $m_l=0.30$ GeV), ($\beta=1.0$ GeV, $m_l=0.24$ GeV), ($\beta=1.0$ GeV, $m_l=0.36$ GeV), respectively. The curves peaking around $\omega=0.4$ GeV(red curves) correspond to the distribution amplitudes $\psi^{QCD}(\omega,u)$, where the solid, dashed-dotted, dashed-double-dotted, dashed-triple-dotted and dashed-quartic-dotted curves correspond to the values of the model parameters ($\epsilon_0=0.20$ GeV, $\epsilon_1=0.65$ GeV), ($\epsilon_0=0.14$ GeV, $\epsilon_1=0.65$ GeV), ($\epsilon_0=0.33$ GeV, $\epsilon_1=0.65$ GeV), ($\epsilon_0=0.20$ GeV, $\epsilon_1=0.35$ GeV), ($\epsilon_0=0.20$ GeV, $\epsilon_1=1.30$ GeV), respectively.

TABLE II: Typical inverse moments defined in Eq. (25) at a fixed energy cut off $\Lambda_{UV}=2.5$ GeV and $\mu=1$ GeV for the two LCDAs $\psi^{QCD}(\omega,u)$ and $\psi^{CQM}(\omega,u)$ discussed in the text.

	$\langle\omega^{-1}\rangle$[GeV^{-1}]	$\langle(\omega u)^{-1}\rangle$[GeV^{-1}]
$\psi^{\rm QCD}(\omega,u)$	$1.66^{+0.72}_{-0.67}$	$5.38^{+2.22}_{-2.07}$
$\psi^{\rm CQM}(\omega,u)$	$1.07^{+1.21}_{-0.15}$	$2.53^{+0.42}_{-0.33}$

distribution amplitudes $\psi^{\rm QCD}(\omega,u)$ and $\psi^{\rm CQM}(\omega,u)$ are compatible with each other within the errors on the model parameters (which are large), with the central values of these moments shifted to lower values for the $\psi^{\rm CQM}(\omega,u)$ LCDA. For the numerical calculations presented here we use $\psi^{\rm CQM}(\omega,u)$ with the quoted errors on the model parameters.

2. Distribution amplitudes of the proton

Similarly, the wave functions of the final state proton has in leading twist the following form [39]

$$(\bar{Y})_{\alpha\beta\gamma}(k_i',\mu) = -\frac{f_N}{8\sqrt{2}N_c}\Big\{[\bar{N}(p')\gamma_5]_\gamma(C^{-1}\not{p}')_{\alpha\beta}\phi^V(k_i',\mu)+[\bar{N}(p')]_\gamma(C^{-1}\gamma_5\not{p}')_{\alpha\beta}\phi^A(k_i',\mu) -[\bar{N}(p')\gamma_5\gamma^\mu]_\gamma(C^{-1}\sigma_{\nu\mu}p'^\nu)_{\alpha\beta}\phi^T(k_i',\mu)\Big\}, \tag{26}$$

Keeping next-to-leading conformal spin, one obtains the following twist-3 distribution amplitudes [21, 40]:

$$\begin{aligned}
\phi^V(x_i,\mu) &= 120x_1x_2x_3\left[\phi_3^0(\mu)+\phi_3^+(\mu)(1-3x_3)\right],\\
\phi^A(x_i,\mu) &= 120x_1x_2x_3(x_2-x_1)\phi_3^-(\mu),\\
\phi^T(x_i,\mu) &= 120x_1x_2x_3\Big[\phi_3^0(\mu)-\frac{1}{2}\left(\phi_3^+-\phi_3^-\right)(\mu)(1-3x_3)\Big].
\end{aligned}$$

Here the moments of the distribution amplitudes for the proton are determined by

$$\phi_3^0=f_N,\quad \phi_3^-=\frac{21}{2}f_N\,A_1^u,\quad \phi_3^+=\frac{7}{2}f_N\,(1-3V_1^d), \tag{27}$$

with all the parameters fixed at the scale $\mu=1$ GeV as

$$\begin{aligned}
|f_N| &= (5.0\pm0.5)\times10^{-3}\mathrm{GeV}^2,\\
A_1^u &= 0.38\pm0.15,\\
V_1^d &= 0.23\pm0.03.
\end{aligned} \tag{28}$$

It is easy to see that the above proton distribution amplitudes satisfy the following relations

$$\begin{aligned}
\phi^V(x_1,x_2,x_3) &= \phi^V(x_2,x_1,x_3),\\
\phi^A(x_1,x_2,x_3) &= -\phi^A(x_2,x_1,x_3),\\
\phi^T(x_1,x_2,x_3) &= \phi^T(x_2,x_1,x_3).
\end{aligned} \tag{29}$$

E. A brief review of the conventional pQCD approach

Factorization of amplitudes is a fundamental tool of QCD perturbative theory to deal with processes involving different energy scales. Based on the k_T factorization, the pQCD approach provides a framework which has been applied to hard exclusive processes. In this approach, hard

gluon(s) exchange is essential to ensure the applicability of the twist expansion, and soft contributions are expected to be less important owing to the suppression by the Sudakov factor. This is the case for the transition form factors involving mesons. We would like to take the $\Lambda_b \to p$ transition form factors as an example, first to illustrate the pQCD factorization theorem, and then offer quantitative estimates for this form factor to check if the soft contributions remain sub-dominant or not in the baryonic transitions.

The factorization theorem states that the transition form factor can be expressed as the convolution of hadronic wave functions ψ_{Λ_b}, ψ_p and the hard scattering amplitude T_H

$$F = \int_0^1 [dx][dx'] \int [d^2\mathbf{k}_T] \int [d^2\mathbf{k}'_T] \psi_p(x', \mathbf{k}'_T, p', \mu) T_H(x, x', M_{\Lambda_b}, \mathbf{k}_T, \mathbf{k}'_T, \mu) \psi_{\Lambda_b}(x, \mathbf{k}_T, p, \mu), \quad (30)$$

which is usually transformed to the impact parameter b space to perform the Sudakov resummation of the double logarithms involved in the radiative corrections to the hadronic wave functions

$$F = \int_0^1 [dx][dx'] \int [d^2\mathbf{b}] \int [d^2\mathbf{b}'] \mathcal{P}_p(x', \mathbf{b}', p', \mu) T_H(x, x', M_{\Lambda_b}, \mathbf{b}, \mathbf{b}', \mu) \mathcal{P}_{\Lambda_b}(x, \mathbf{b}, p, \mu). \quad (31)$$

Here $\mathcal{P}_{\Lambda_b}(x, \mathbf{b}, p, \mu)$ and $\mathcal{P}_p(x', \mathbf{b}', p', \mu)$ are the Fourier transforms of the $\psi_{\Lambda_b}(x, \mathbf{k}_T, p, \mu)$ and $\bar{\psi}_p(x', \mathbf{k}'_T, p', \mu)$, respectively. Radiative corrections to the hadronic wave function can generate a soft logarithm $\alpha_s \ln(Qb)$, whose overlap with the original collinear logarithm leads to a double logarithm $\alpha_s \ln^2(Qb)$. This type of large logarithm must be organized in order to ensure the validity of the perturbative expansion. Resummation techniques have been developed to deal with such double logarithms. The result is a Sudakov exponential $\exp[-s(Q, b)]$, which decreases fast with increasing b and vanishes at $b = 1/\Lambda_{QCD}$.

The expressions for the Sudakov evolution of the hadronic wave functions $\mathcal{P}_{\Lambda_b}(x, \mathbf{b}, p, \mu)$ and $\mathcal{P}_p(x', \mathbf{b}', p', \mu)$ can be expressed as products of the Sudakov exponents $s(b, Q)$ and reduced hadronic wave functions, denoted by $\tilde{\mathcal{P}}_{\Lambda_b}(x, \mathbf{b}, p, \mu)$ and $\tilde{\mathcal{P}}_p(x', \mathbf{b}', p', \mu)$:

$$\begin{aligned} \mathcal{P}_{\Lambda_b}(x, \mathbf{b}, p, \mu) &= \exp\left[-\sum_{i=2}^{3} s(w, k_i^+)\right] \tilde{\mathcal{P}}_{\Lambda_b}(x, \mathbf{b}, p, \mu) \,, \\ \mathcal{P}_p(x', \mathbf{b}', p', \mu) &= \exp\left[-\sum_{i=1}^{3} s(w', k_i'^-)\right] \tilde{\mathcal{P}}_p(x', \mathbf{b}', p', \mu), \end{aligned} \quad (32)$$

where $s(b, Q)$ is defined as

$$\begin{aligned} s(b, Q) \;=\; & \frac{A^{(1)}}{2\beta_1} \hat{q} \ln\left(\frac{\hat{q}}{\hat{b}}\right) - \frac{A^{(1)}}{2\beta_1}\left(\hat{q} - \hat{b}\right) + \frac{A^{(2)}}{4\beta_1^2}\left(\frac{\hat{q}}{\hat{b}} - 1\right) - \left[\frac{A^{(2)}}{4\beta_1^2} - \frac{A^{(1)}}{4\beta_1} \ln\left(\frac{e^{2\gamma_E - 1}}{2}\right)\right] \ln\left(\frac{\hat{q}}{\hat{b}}\right) \\ & + \frac{A^{(1)}\beta_2}{4\beta_1^3} \hat{q} \left[\frac{\ln(2\hat{q}) + 1}{\hat{q}} - \frac{\ln(2\hat{b}) + 1}{\hat{b}}\right] + \frac{A^{(1)}\beta_2}{8\beta_1^3} \left[\ln^2(2\hat{q}) - \ln^2(2\hat{b})\right], \end{aligned} \quad (33)$$

with

$$\hat{q} \equiv \ln[Q/(\sqrt{2}\Lambda)], \quad \hat{b} \equiv \ln[1/(b\Lambda)], \tag{34}$$

and the coefficients $A^{(i)}$ and β_i are

$$\begin{aligned} \beta_1 = \frac{33-2n_f}{12}, \quad \beta_2 = \frac{153-19n_f}{24}, \\ A^{(1)} = \frac{4}{3}, \quad A^{(2)} = \frac{67}{9} - \frac{\pi^2}{3} - \frac{10}{27}n_f + \frac{8}{3}\beta_1 \ln(\frac{1}{2}e^{\gamma_E}), \end{aligned} \tag{35}$$

n_f is the number of quark flavors and γ_E is the Euler constant. We will use the one-loop running coupling constant, i.e. we pick up the first four terms in the expression for the function $s(Q,b)$.

Apart from the double logarithms due to the inclusion of the transverse momentum, large single logarithms from ultraviolet divergences can also emerge in the radiative corrections to both the hadronic wave functions and the hard kernels, which are summed by the renormalization group (RG) method

$$\left[\mu\frac{\partial}{\partial\mu} + \beta(g)\frac{\partial}{\partial g}\right] \tilde{\mathcal{P}}_{\Lambda_b}(x,\mathbf{b},p,\mu) = -\frac{8}{3}\gamma_q \tilde{\mathcal{P}}_{\Lambda_b}(x,\mathbf{b},p,\mu), \tag{36}$$

$$\left[\mu\frac{\partial}{\partial\mu} + \beta(g)\frac{\partial}{\partial g}\right] \tilde{\mathcal{P}}_{p}(x',\mathbf{b}',p',\mu) = -3\gamma_q \tilde{\mathcal{P}}_{p}(x',\mathbf{b}',p',\mu), \tag{37}$$

$$\left[\mu\frac{\partial}{\partial\mu} + \beta(g)\frac{\partial}{\partial g}\right] T_H(x,x',M_{\Lambda_b},\mathbf{b},\mathbf{b}',\mu) = \frac{17}{3}\gamma_q T_H(x,x',M_{\Lambda_b},\mathbf{b},\mathbf{b}',\mu). \tag{38}$$

Here the quark anomalous dimension in the axial gauge is $\gamma_q = -\alpha_s/\pi$. In terms of the above equations, we can get the RG evolution of the hadronic wave functions and hard scattering amplitude as

$$\begin{aligned} \tilde{\mathcal{P}}_{\Lambda_b}(x,\mathbf{b},p,\mu) &= \exp\left[-\frac{8}{3}\int_{\kappa w}^{\mu}\frac{d\bar{\mu}}{\bar{\mu}}\gamma_q(\alpha_s(\bar{\mu}))\right] \times \tilde{\mathcal{P}}_{\Lambda_b}(x,\mathbf{b},p,w), \\ \tilde{\mathcal{P}}_{p}(x',\mathbf{b}',p',\mu) &= \exp\left[-3\int_{\kappa w'}^{\mu}\frac{d\bar{\mu}}{\bar{\mu}}\gamma_q(\alpha_s(\bar{\mu}))\right] \times \tilde{\mathcal{P}}_{p}(x',\mathbf{b}',p',w'), \\ T_H(x,x',M_{\Lambda_b},\mathbf{b},\mathbf{b}',\mu) &= \exp\left[-\frac{17}{3}\int_{\mu}^{t}\frac{d\bar{\mu}}{\bar{\mu}}\gamma_q(\alpha_s(\bar{\mu}))\right] \times T_H(x,x',M_{\Lambda_b},\mathbf{b},\mathbf{b}',t)\ , \end{aligned} \tag{39}$$

The factorization scales w and w' represent the inverse of a typical transverse distance among the three valence quarks of the initial and final states. The choices of w and w' are

$$w = \min(\frac{1}{b_1},\frac{1}{b_2},\frac{1}{b_3}), \qquad w' = \min(\frac{1}{b_1'},\frac{1}{b_2'},\frac{1}{b_3'}), \tag{40}$$

with the variables b_1 and b_1' defined as

$$b_1 = |\mathbf{b_2} - \mathbf{b_3}|, \qquad b_1' = |\mathbf{b_2}' - \mathbf{b_3}'|, \tag{41}$$

with the other b_is and b_i's defined by permutation. The introduction of the parameter κ is done from the viewpoint of the resummation, since the scale $\kappa w^{(\prime)}$, with κ of order unity, is equivalent to $w^{(\prime)}$ within the accuracy of the next-to-leading logarithms [41]. The variation of κ represents different partitions of the radiative corrections to the perturbative Sudakov factor and the non-perturbative wave function. The best fit to the experimental data of the proton form factor determines the parameter as $\kappa = 1.14$ [13].

Furthermore, loop corrections for the weak vertex can also give rise to another type of double logarithms $\alpha_s \ln^2 x_i$, which are usually factorized from the hard amplitude and resummed into the jet function $S_t(x_i)$ to smear the end-point singularity. It should be pointed out that the Sudakov factor from threshold resummation is process-independent, and hence universal [42]. The following approximate parametrization is proposed in Ref. [43] for phenomenological applications

$$S_t(x) = \frac{2^{1+2c}\Gamma(3/2+c)}{\sqrt{\pi}\Gamma(1+c)}[x(1-x)]^c \,, \tag{42}$$

with the parameter $c \simeq 0.3$ determined from the best fit to the next-to-leading-logarithm threshold resummation in moment space. The threshold factor modifies the end-point behavior of the hadronic distribution amplitudes and forces them to vanish faster as $x \to 0$. Collecting everything together, we arrive at the typical expression for the factorization formula of the form factor in the pQCD approach

$$\begin{aligned} F &= \int_0^1 [dx] \int [dx'] \int [d^2\mathbf{b}] \int [d^2\mathbf{b}'] \bar{\tilde{\mathcal{P}}}_p(x', \mathbf{b}', p', w') T_H(x, x', M_{\Lambda_b}, \mathbf{b}, \mathbf{b}', t) \tilde{\mathcal{P}}_{\Lambda_b}(x, \mathbf{b}, p, w) S_t(x^{(\prime)}) \\ &\quad \times \exp\left[-\sum_{i=2}^{3} s(w, k_i^+) - \frac{8}{3}\int_{\kappa w}^{t} \frac{d\bar{\mu}}{\bar{\mu}} \gamma_q(\alpha_s(\bar{\mu})) - \sum_{i=1}^{3} s(w', k_i'^-) - 3\int_{\kappa w'}^{t} \frac{d\bar{\mu}}{\bar{\mu}} \gamma_q(\alpha_s(\bar{\mu})) \right] . \end{aligned} \tag{43}$$

Apart from the hard perturbative kernel $T_H(x, x', ...)$, the same expression holds for the mesonic and baryonic transition form factors. As we shall see quantitatively below, the hard perturbative kernels entering the latter are parametrically suppressed compared to the former. Physical interpretation of the Sudakov factor is well known [44], namely it is a probability distribution function for emitting no soft gluons. When a quark is accelerated in QCD, infinitely many gluons are emitted. Hence, we may observe many hadrons (or jets) at the end if gluonic bremsstrahlung occurs. Therefore, the amplitude for an exclusive decay Λ_b to a light baryon and a light meson is proportional to the probability that no bremsstrahlung gluon is emitted. This is just the role of the Sudakov factor in the k_T factorization. It is known that the Sudakov factor is large only for small transverse intervals between the quarks in the hadron. A large transverse interval implies that the quarks in the hadron are separated and hence less color shielded. Thus the Sudakov factor suppresses the long distance contributions for the decay amplitude.

III. CALCULATIONS OF BARYONIC DECAYS $\Lambda_b \to p\pi,\ pK$ IN THE PQCD APPROACH

Topological diagrams responsible for the decay of Λ_b to a light baryon and a light meson are presented in Fig. 3. In terms of the hard-scattering mechanism, the exchange of two hard gluons is needed to ensure that the light spectator quarks in the initial states turn out as collinear objects in the final state. With this, the various diagrams for the $\Lambda_b \to p\pi$ decays in the pQCD approach in the lowest order are displayed in Appendix B. Fig. 4 shows the external W emission diagrams, Fig. 5 the internal W emission diagrams, Fig. 6 the W exchange diagrams, Fig. 7 the bow-tie diagrams and Fig. 8 the penguin diagrams. We also include diagrams containing the three-gluon-vertex displayed in Fig. 9. Their contribution is, however, about an order of magnitude smaller than that from the external W emission (T) diagrams, but it can be comparable to that of the internal W emission (C) diagrams. As for $\Lambda_b \to pK$ decay, only Figs. 4, 7, 8, and 9 contribute to the decay amplitude.

A. General factorization formulae for $\Lambda_b \to p\pi,\ pK$ decays

The $\Lambda_b \to p\pi,\ pK$ decay amplitude $\mathcal{M}$ is decomposed into two different structures with the corresponding coefficients f_1 and f_2:

$$\mathcal{M} = \bar{p}(p')[f_1 + f_2\gamma_5]\Lambda_b(p). \tag{44}$$

using the equation of motion for a free Dirac particle. Similar to the factorization formula for the form factors of the $\Lambda_b \to p$ transition, the coefficients $f_i (i = 1, 2)$ can be expressed as

$$\begin{aligned} f_i^j &= G_F \frac{\pi^2}{144\sqrt{3}} f_{\Lambda_b} f_p \sum_{m=V,A,T}^{n=A,P,T} \int [\mathcal{D}x] \int [\mathcal{D}b]^j [\alpha_s(t^j)]^2 a^j(t^j) \psi_{\Lambda_b}(x) \psi_p^m(x') \phi_M^n(y) H_i^{mnj}(x, x', y) \\ &\quad \times \Omega^j(b, b', b_q) \exp[-S^j]. \end{aligned} \tag{45}$$

Here, f_i^j $(i = 1, 2)$ denotes the contribution to the coefficient f_i by the "j_{th}" diagram displayed in Fig. 4-9, and a^j are the corresponding Wilson coefficients. The hard function $\Omega^j(b, b', b_q)$ arises from the Fourier transformation of the denominators of the internal particle propagators in the jth diagram. The hard amplitudes $H_i^{mnj}(x, x', y)$ depend on the spin structures of the three valence quarks in the proton and the form factors $f_{1,2}$. The integration measure involving the momentum fractions can be written as

$$[\mathcal{D}x] = [dx][dx']dy, \quad [dx] = dx_1 dx_2 dx_3 \delta(1 - \sum_{i=1}^{3} x_i), \quad [dx'] = dx_1' dx_2' dx_3' \delta(1 - \sum_{i=1}^{3} x_i'), \tag{46}$$

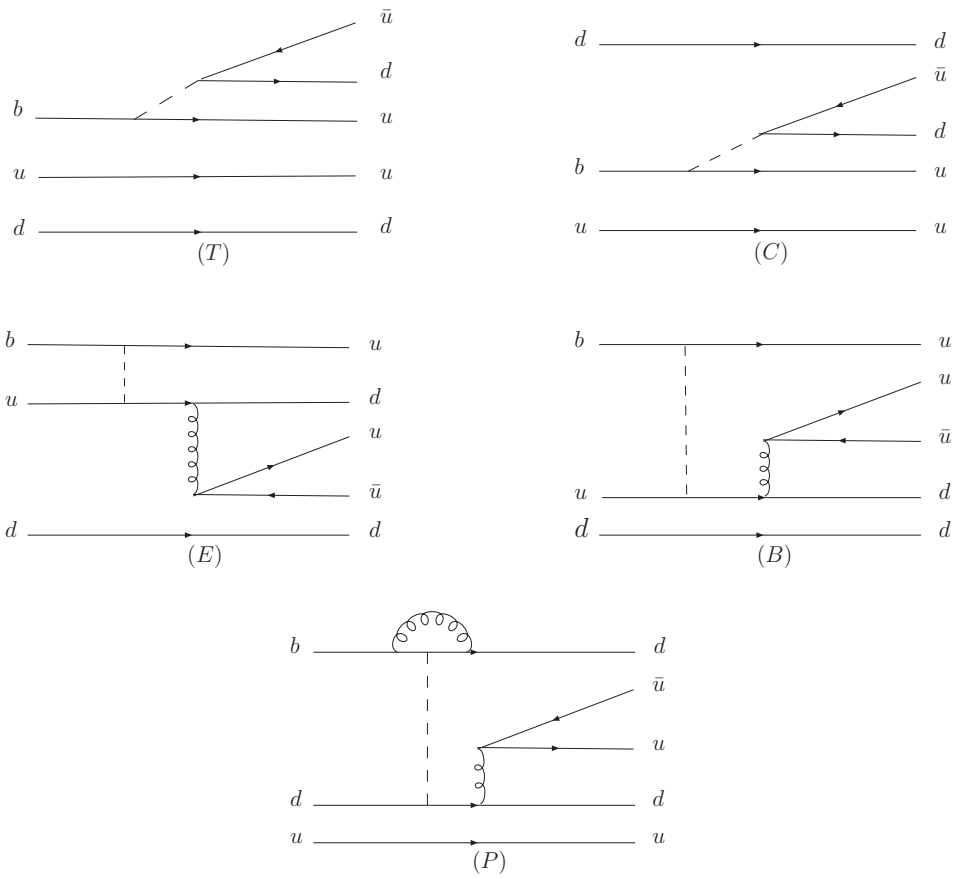

FIG. 3: Topological diagrams responsible for the decay $\Lambda_b \to p\pi$, where T denotes the external W emission diagram; C represents the internal W emission diagram; E labels W exchange diagram; B denotes the diagram that can be obtained from the E type diagram by exchanging the two identical down quarks in the final states; and P represents the diagram that can only be induced by the penguin operators.

and the expressions for the measure of the transverse extent $[\mathcal{D}b]$ will be shown in the factorization formulae given in Appendix B.

The exponents S^j in the Sudakov factor are determined for the factorizable diagrams by

$$S^j(x,x',b,b') = \sum_{i=2}^{3} s(w,k_i^+) + \frac{8}{3}\int_{\kappa w}^{t_j}\frac{d\bar{\mu}}{\bar{\mu}}\gamma_q(\alpha_s(\bar{\mu})) + \sum_{i=1}^{3} s(w',k_i'^-) + 3\int_{\kappa w'}^{t_j}\frac{d\bar{\mu}}{\bar{\mu}}\gamma_q(\alpha_s(\bar{\mu}))\ , \quad (47)$$

and for the non-factorizable diagrams by

$$\begin{aligned} S^j(x,x',y,b,b',b_q) \ =\ & \sum_{i=2}^{3} s(w,k_i^+) + \frac{8}{3}\int_{\kappa w}^{t_j}\frac{d\bar{\mu}}{\bar{\mu}}\gamma_q(\alpha_s(\bar{\mu})) + \sum_{i=1}^{3} s(w',k_i'^-) + 3\int_{\kappa w'}^{t_j}\frac{d\bar{\mu}}{\bar{\mu}}\gamma_q(\alpha_s(\bar{\mu})) \\ & + \sum_{i=1}^{2} s(w_q,q_i^+) + 2\int_{w_q}^{t_j}\frac{d\bar{\mu}}{\bar{\mu}}\gamma_q(\alpha_s(\bar{\mu}))\ , \end{aligned} \quad (48)$$

where t^j is the typical energy scale of the "j_{th}" diagram and is chosen as

$$t^j = max(t_1^j, t_2^j, t_3^j, t_4^j, w, w', w_q), \quad (49)$$

TABLE III: The coefficients f_1 and f_2 contributed by the Feynman diagrams with definite topologies in the $\Lambda_b \to p\pi$ decay based on the conventional pQCD approach.

	f_1	f_2
T	$-2.42\times10^{-9}-i2.07\times10^{-9}$	$-1.74\times10^{-9}-i1.22\times10^{-9}$
C	$2.05\times10^{-10}-i4.60\times10^{-10}$	$-2.35\times10^{-10}+i4.77\times10^{-10}$
E	$2.89\times10^{-11}-i8.95\times10^{-12}$	$1.11\times10^{-11}-i4.36\times10^{-12}$
B	$-7.00\times10^{-11}+i3.33\times10^{-10}$	$2.21\times10^{-10}-i4.04\times10^{-11}$
P	$-6.84\times10^{-12}+i4.85\times10^{-11}$	$7.00\times10^{-12}-i4.75\times10^{-11}$
G	$1.37\times10^{-10}+i1.71\times10^{-11}$	$-1.60\times10^{-10}+i2.01\times10^{-10}$

where the hard scales t_1^j, t_2^j are relevant to the two virtual quarks, and t_3^j, t_4^j are associated with the two hard gluons. w and w' have been given in Eq. (40) and $w_q = 1/b_q$. The maximum in the above choice simply indicates that the hard scales should be larger than the factorization scales.

The factorization formulae for some typical diagrams corresponding to different topologies in the $\Lambda_b \to p\pi$ decay are given in Appendix B. The corresponding factorization formulae for $\Lambda_b \to pK$ decay can be obtained directly following the same rules.

B. Numerical results for $\Lambda_b \to p\pi,\ pK$ decays

For the CKM matrix elements, we use as input the updated results from [45] and drop the (small) errors on V_{ud}, V_{us} and V_{tb}:

$$\begin{aligned}
&|V_{ud}| = 0.974, && |V_{us}| = 0.225, && |V_{ub}| = (3.50^{+0.15}_{-0.14})\times10^{-3},\\
&|V_{td}| = (8.59^{+0.27}_{-0.29})\times10^{-3}, && |V_{ts}| = (40.41^{+0.38}_{-1.15})\times10^{-3}, && |V_{tb}| = 0.999,\\
&\beta = (21.58^{+0.91}_{-0.81})^\circ, && \gamma = (67.8^{+4.2}_{-3.9})^\circ.
\end{aligned} \tag{50}$$

It will be shown that the CKM factors mostly yield an overall factor for the branching ratios and do not introduce large uncertainties to the numerical results.

We start by discussing the numerical results in the conventional pQCD approach. To that end, we list the coefficients f_1 and f_2 defined in Eq. (44) contributed by the Feynman diagrams with different topologies in the $\Lambda_b \to p\pi$ decay in Table III. From this table, we observe that the amplitudes satisfy the relations $T \gg C \gg E$.

As mentioned earlier, the T type diagrams dominate the $\Lambda_b \to p\pi$ decays. For this case we present the factorizable and non-factorizable contributions in the $\Lambda_b \to p\pi$ decays in Table IV.

TABLE IV: The coefficients f_1 and f_2 in the $\Lambda_b \to p\pi,\ pK$ decays from the factorizable and non-factorizable external W emission (T) diagrams in the conventional pQCD approach.

	factorizable	non-factorizable
$f_1(\Lambda_b \to p\pi)$	$1.47 \times 10^{-11} - i1.97 \times 10^{-11}$	$-2.43 \times 10^{-9} - i2.05 \times 10^{-9}$
$f_2(\Lambda_b \to p\pi)$	$1.26 \times 10^{-11} - i1.94 \times 10^{-11}$	$-1.75 \times 10^{-9} - i1.20 \times 10^{-9}$
$f_1(\Lambda_b \to pK)$	$-1.52 \times 10^{-11} - i0.62 \times 10^{-11}$	$-0.88 \times 10^{-9} + i0.54 \times 10^{-10}$
$f_2(\Lambda_b \to pK)$	$0.17 \times 10^{-11} - i0.60 \times 10^{-11}$	$-1.06 \times 10^{-9} + i1.67 \times 10^{-9}$

We observe that the factorizable contribution is approximately two orders of magnitude smaller than the non-factorizable contribution. This is also the reason that the the conventional pQCD predictions for the semileptonic decay $\Lambda_b \to pl\bar{\nu}$ [39] and the radiative decay $\Lambda_b \to \Lambda\gamma$ [17] are much smaller than those evaluated in other theoretical frameworks (such as the constituent quark model or the QCD sum rules).

The suppression of the factorizable contributions in the conventional pQCD approach has been observed also in the analysis of the $\Lambda_b \to \Lambda J/\psi$ decays [31], where the non-factorizable contributions are also found almost two orders of magnitude larger than those from the factorizable diagrams. In order to understand the large contribution of the non-factorizable diagrams in Λ_b decays, it is necessary to recall the role of the Sudakov factor in the k_T factorization approach. As stated in section II, the Sudakov factor can only suppress the region with large b's corresponding to small k_T's, and has almost no effect in the region where the transverse momentum k_T is large. Taking the non-factorizable diagram T_{25} as an example, the two virtual quarks can be on the mass shell even in the region with large k_T. Therefore, this diagram is not subjected to the suppression from the Sudakov factor. It is then expected that the amplitudes for the non-factorizable diagrams should be much larger than those from the factorizable diagrams, where the two virtual quarks can be on the mass shell only in the small k_T region. Actually, a similar case also occurs in the hadronic B meson decays. There, the annihilation diagrams contributing to the $B \to M_1 M_2$ decays in the pQCD approach is very important, which is responsible for the large CP violation and the enhancement of the transverse polarization fractions predicted in the k_T factorization. The large contribution from the annihilation diagrams in the pQCD approach is due to the fact that the inner quark can be on the mass shell in the region of large k_T. The numerical analysis also shows that the six non-factorizable diagrams $T_{19}, T_{20}, T_{21}, T_{25}, T_{31}, T_{32}$ play the most significant role in the decay amplitude for the $\Lambda_b \to p\pi$ transition.

TABLE V: The form factor g_1 responsible for the $\Lambda_b \to p$ transition at zero momentum transfer, calculated by us (this work) and in the non-relativistic quark model (NRQM), LCSR, and in another pQCD approach. The uncertainties from the variations of the hard scale, Λ_{QCD} and the shape parameter β in the Λ_b wave functions have been combined together in our work.

	NRQM [19]	LCSR (full QCD)[23]	pQCD [14]	pQCD (this work)
g_1	0.043	0.018	2.3×10^{-3}	$2.2^{+0.8}_{-0.5} \times 10^{-3}$

We consider the smallness of the factorizable contributions in the conventional pQCD approach as unrealistic. Consequently, we argue that the $\Lambda_b \to p$ transition form factors can not be reliably calculated in the perturbative k_T scheme, i.e. these form factors are dominated by non-perturbative soft contributions, which can not be estimated in the pQCD approach. Of course, this could easily be checked by measuring the semileptonic Λ_b decays $\Lambda_b \to p\ell\bar{\nu}_\ell$, which depend only on the factrorizable diagrams. Pending this determination, we consider it as a more reasonable approach to calculate the $\Lambda_b \to p$ transition form factor by means of some non-perturbative method.

The form factors of $\Lambda_b \to p$ transition are defined as

$$\langle p(p')|\bar{u}\gamma_\mu b|\Lambda_b(p)\rangle \;=\; \overline{p}(p')(g_1\gamma_\mu + g_2 i\sigma_{\mu\nu}q^\nu + g_3 q_\mu)\Lambda_b(p), \tag{51}$$

where all the form factors g_i are functions of the square of momentum transfer q^2. We show in Table V numerical values for the vector transition form factor g_1 for the $\Lambda_b \to p$ transition. These results are obtained in the non-relativistic quark model (NRQM) [19], LCSR [23], an earlier pQCD calculation [14], and this work (also a pQCD calculation) for comparison. From this Table we see that the predictions for the transition form factor g_1 are scattered, with the NRQM [19] and the LCSR [23] values differing by a factor 2, but the two conventional pQCD results shown, while consistent with each other, are smaller from those obtained using the non-perturbative methods typically by an order of magnitude.

To understand the marked difference of the form factor g_1 predicted in the pQCD approach and in the other frameworks, we recall that the hard dynamics is assumed to be dominant in the heavy-to-light transition form factors in the former and the soft contribution, which is not calculable, is assumed to be less important due to the Sudakov resummation. Table V suggests that the soft dynamics in the heavy-to-light transition form factors is the dominant effect, in all likelihood overwhelming the mechanism of the hard gluon exchange for the baryonic transitions. Similar large soft contributions have been also observed in the nonleptonic charmed meson decays

[46] as well as in the semileptonic $\Lambda_b \to \Lambda\gamma,\ \Lambda l^+ l^-$ decays [17, 33]. It is found in [33] that the hard contributions to the $\Lambda_b \to \Lambda$ form factors are almost an order of magnitude smaller than that those from the soft contributions.

In the modified version of the pQCD approach, which we call *hybrid* pQCD, the form factors are taken as external inputs. The perturbative correction to the factorizable amplitude will then enter through the Wilson coefficients, which are known in next-to-next-to-leading order (NNLO), and the vertex corrections, which have been recently calculated for the tree diagrams in the charmless hadronic B decays in NNLO [47, 48]. As the complete NNLO corrections, including the QCD penguin amplitudes, are still not yet at hand, we follow the approximate (and less precise) approach proposed in Ref. [49] to neglect the vertex corrections and vary the renormalization scale μ of the Wilson coefficients between $0.5m_b$ and $1.5m_b$. Surely, this step of the calculation can be systematically improved once the complete NNLO virtual corrections are available. The non-factorizable contributions will be evaluated as already discussed in the conventional pQCD approach.

Following the above procedure, we write the complete decay amplitude for $\Lambda_b \to p\pi,\ pK$ as

$$\begin{aligned}\mathcal{M}(\Lambda_b \to p\pi) &= \mathcal{M}_f(\Lambda_b \to p\pi) + \mathcal{M}_{nf}(\Lambda_b \to p\pi)\\ \mathcal{M}(\Lambda_b \to pK) &= \mathcal{M}_f(\Lambda_b \to pK) + \mathcal{M}_{nf}(\Lambda_b \to pK),\end{aligned} \tag{52}$$

where $\mathcal{M}_{nf}(\Lambda_b \to p\pi)$ and $\mathcal{M}_{nf}(\Lambda_b \to pK)$ denote the contributions from the non-factorizable diagrams and have been computed in the conventional pQCD approach. To calculate the factorizable amplitudes $\mathcal{M}_f(\Lambda_b \to p\pi)$ and $\mathcal{M}_f(\Lambda_b \to pK)$, we first need to deal with the hadronic matrix elements with the insertion of $(V-A)\otimes(V+A)$ operators, i.e.,the $O_5 - O_8$ penguin operators. Making use of the Fierz identity, the factorization assumption and the Dirac equation, the matrix element of the operator O_6 can be written as

$$\langle pM|O_6|\Lambda_b\rangle = [R_1^M\langle p|\bar{q'}\gamma_\mu b|\Lambda_b\rangle + R_2^M\langle p|\bar{q'}\gamma_\mu\gamma_5 b|\Lambda_b\rangle]\langle M|\bar{q}\gamma_\mu(1-\gamma_5)q'|0\rangle \tag{53}$$

with

$$R_1^M = \frac{2m_M^2}{(m_b - m_u)(m_u + m_q)}, \qquad R_2^M = \frac{2m_M^2}{(m_b + m_u)(m_u + m_q)}, \tag{54}$$

where the quark masses are the current quark masses. In addition to the form factors defined in Eq. (51), we need the matrix element describing the $\Lambda_b \to p$ transition induced by the axial-vector current

$$\langle\Lambda(P)|\bar{s}\gamma_\mu\gamma_5 b|\Lambda_b(P+q)\rangle = \overline{\Lambda}(P)(G_1\gamma_\mu + G_2 i\sigma_{\mu\nu}q^\nu + G_3 q_\mu)\gamma_5\Lambda_b(P+q). \tag{55}$$

TABLE VI: Numerical values of the form factors g_1 and $m_{\Lambda_b} g_2$ at zero momentum transfer, responsible for the $\Lambda_b \to p$ transition, estimated in the LCSR approach [23].

form factors	g_1	$m_{\Lambda_b} g_2$
$\Lambda_b \to p$	0.018	-0.159

It is then straightforward to write the factorizable amplitudes $\mathcal{M}_f(\Lambda_b \to p\pi)$ and $\mathcal{M}_f(\Lambda_b \to pK)$ as

$$\begin{aligned}
&\mathcal{M}_f(\Lambda_b \to p\pi) \\
&= \frac{G_F}{\sqrt{2}} f_\pi \bar{p}(p') \Big\{ \Big[V_{ub}V_{ud}^* a_1 - V_{tb}V_{td}^* (a_4 + a_{10} + R_1^\pi (a_6 + a_8)) \Big] \Big[g_1(m_\pi^2)(M_{\Lambda_b} - M_p) + g_3(m_\pi^2) m_\pi^2 \Big] \\
&+ \Big[V_{ub}V_{ud}^* a_1 - V_{tb}V_{td}^* (a_4 + a_{10} - R_2^\pi (a_6 + a_8)) \Big] \Big[G_1(m_\pi^2)(M_{\Lambda_b} + M_p) - G_3(m_\pi^2) m_\pi^2 \Big] \gamma_5 \Big\} \Lambda_b(p), \qquad (56) \\
&\mathcal{M}_f(\Lambda_b \to pK) \\
&= \frac{G_F}{\sqrt{2}} f_K \bar{p}(p') \Big\{ \Big[V_{ub}V_{us}^* a_1 - V_{tb}V_{ts}^* (a_4 + a_{10} + R_1^K (a_6 + a_8)) \Big] \Big[g_1(m_K^2)(M_{\Lambda_b} - M_p) + g_3(m_K^2) m_K^2 \Big] \\
&+ \Big[V_{ub}V_{us}^* a_1 - V_{tb}V_{ts}^* (a_4 + a_{10} - R_2^K (a_6 + a_8)) \Big] \Big[G_1(m_K^2)(M_{\Lambda_b} + M_p) - G_3(m_K^2) m_K^2 \Big] \gamma_5 \Big\} \Lambda_b(p). \qquad (57)
\end{aligned}$$

The masses of the pseudoscalar mesons of π and K can safely be neglected, therefore only the form factors at the zero-momentum transfer will be involved in the numerical computations.

To evaluate the $\Lambda_b \to p\pi,\ pK$ decays numerically, we need to specify the form factors responsible for the $\Lambda_b \to p$ transition. As can be seen from Eqs. (56-57), the form factors g_3 and G_3, whose contributions are proportional to the mass of the corresponding meson, are inessential for the calculation of the decay amplitudes. In view of the minor effects of these two form factors, it is quite adequate to determine them in terms of the relations derived in the heavy quark limit. As is well known, the form factors g_i and G_i satisfy

$$g_1 = G_1 = \xi_1 + \frac{m_\Lambda}{m_{\Lambda_b}} \xi_2, \qquad (58)$$

$$g_2 = G_2 = g_3 = G_3 = \frac{\xi_2}{m_{\Lambda_b}}. \qquad (59)$$

in the heavy quark effective theory (HQET), where the two independent form factors ξ_1 and ξ_2 are defined as

$$\langle \Lambda(P) | \bar{b} \Gamma s | \Lambda_b(P+q) \rangle = \overline{\Lambda}(P) [\xi_1(q^2) + \not{v} \xi_2(q^2)] \Gamma \Lambda_b(P+q), \qquad (60)$$

with Γ being an arbitrary Lorentz structure and v_μ being the four-velocity of the Λ_b baryon. An analysis of the form factors g_i and G_i has been performed in the LCSR [23], which we shall use

TABLE VII: The coefficients f_1 and f_2 in the decays $\Lambda_b \to p\pi,\ pK$ contributed by the factorizable and non-factorizable external W emission (T) diagrams in the hybrid pQCD scheme.

	factorizable	non-factorizable
$f_1(\Lambda_b \to p\pi)$	$2.43 \times 10^{-10} - i4.39 \times 10^{-10}$	$-2.43 \times 10^{-9} - i2.05 \times 10^{-9}$
$f_2(\Lambda_b \to p\pi)$	$2.64 \times 10^{-10} - i6.54 \times 10^{-10}$	$-1.75 \times 10^{-9} - i1.20 \times 10^{-9}$
$f_1(\Lambda_b \to pK)$	$-3.17 \times 10^{-10} - i1.22 \times 10^{-10}$	$-0.88 \times 10^{-9} + i0.54 \times 10^{-10}$
$f_2(\Lambda_b \to pK)$	$1.74 \times 10^{-10} - i1.96 \times 10^{-10}$	$-1.06 \times 10^{-9} + i1.67 \times 10^{-9}$

here. The numerical results for g_1 and $m_{\Lambda_b} g_2$ needed for our numerical calculations are grouped in Table VI, which correspond to $\xi_1 = 0.050$ and $\xi_2 = -0.16$.

Utilizing the Wilson coefficients, the input form factors just discussed and the CKM factors given earlier, we can now compute the factorizable contributions to f_1 and f_2 in the hybrid pQCD approach and compare them to the corresponding non-factorizable contributions, which have been given already earlier. The results are given in Table VII. From this table we see that the factorizable contributions are now much larger than in the conventional pQCD approach, though they are still smaller than the corresponding non-factorizable contributions.

We are now in a position to present our final results concerning the branching ratios, direct CP asymmetries and the polarization asymmetry parameter α for the two decay channels in the conventional pQCD and in the hybrid pQCD approach. The CP-asymmetry $A_{\rm CP}(\Lambda_b^0 \to p\pi^-)$ is defined as follows:

$$A_{\rm CP}(\Lambda_b^0 \to p\pi^-) \equiv \frac{\mathcal{B}(\bar{\Lambda}_b^0 \to \bar{p}\pi^+) - \mathcal{B}(\Lambda_b^0 \to p\pi^-)}{\mathcal{B}(\bar{\Lambda}_b^0 \to \bar{p}\pi^+) + \mathcal{B}(\Lambda_b^0 \to p\pi^-)}\,, \tag{61}$$

with $A_{\rm CP}(\Lambda_b^0 \to pK^-)$ defined similarly. The asymmetry parameter α associated with the anisotropic angular distribution of the proton emitted in the polarized Λ_b baryon decays is defined as follows:

$$\Gamma = \Gamma_0(1 + \alpha \mathbf{p} \cdot \mathbf{s_{\Lambda_b}}) \tag{62}$$

with $\mathbf{p}$, $\mathbf{s_{\Lambda_b}}$ being the three-momentum and spin vector of the proton in the rest frame of the Λ_b baryon. The explicit expression of α can be written as [50]

$$\alpha = -\frac{2\tilde{\kappa} Re(f_1^* f_2)}{(|f_1|^2 + \tilde{\kappa}^2 |f_2|^2)}\,, \tag{63}$$

with $\tilde{\kappa} = |\mathbf{p}|/(E_p + m_p) = \sqrt{(E_p + m_p)/(E_p - m_p)}$.

TABLE VIII: The CP-averaged branching ratios, direct CP asymmetries and the polarization asymmetry parameter α for the $\Lambda_b \to p\pi, pK$ decays obtained in the conventional and the hybrid pQCD approaches. The errors for these entries correspond to the uncertainties in the input hadronic quantities, the scale-dependence, and the CKM matrix elements, respectively. Current experimental measurements at the Tevatron [24] are also listed.

	pQCD (conventional)	pQCD (hybrid scheme)	Exp.
$\mathcal{B}(\Lambda_b \to p\pi)$	$4.66^{+2.08+0.70+0.35}_{-1.74-0.35-0.35} \times 10^{-6}$	$5.21^{+2.42+0.30+0.42}_{-1.89-0.10-0.37} \times 10^{-6}$	$3.5 \pm 0.6 \pm 0.9 \times 10^{-6}$
$\mathcal{B}(\Lambda_b \to pK)$	$1.82^{+0.74+0.62+0.07}_{-0.71-0.80-0.05} \times 10^{-6}$	$2.02^{+0.78+0.55+0.10}_{-0.86-0.90-0.05} \times 10^{-6}$	$5.6 \pm 0.8 \pm 1.5 \times 10^{-6}$
$A_{\rm CP}(\Lambda_b \to p\pi)$	$-0.32^{+0.27+0.41+0.01}_{-0.00-0.00-0.01}$	$-0.31^{+0.28+0.32+0.01}_{-0.00-0.00-0.01}$	$-0.03 \pm 0.17 \pm 0.05$
$A_{\rm CP}(\Lambda_b \to pK)$	$-0.03^{+0.21+0.13+0.00}_{-0.00-0.04-0.00}$	$-0.05^{+0.26+0.03+0.01}_{-0.00-0.05-0.00}$	$-0.37 \pm 0.17 \pm 0.03$
$\alpha(\Lambda_b \to p\pi)$	$-0.83^{+0.03+0.03+0.01}_{-0.01-0.07-0.01}$	$-0.84^{+0.03+0.00+0.01}_{-0.00-0.00-0.01}$	—
$\alpha(\Lambda_b \to pK)$	$0.03^{+0.00+0.00+0.03}_{-0.36-0.07-0.05}$	$0.08^{+0.00+0.05+0.04}_{-0.38-0.42-0.04}$	—

We present our results in the two pQCD approaches and compare them with the current experimental data from the Tevatron [24] in Table VIII. The first error in the pQCD-based entries arises from the input hadronic parameters, which is dominated by the errors on the normalization constant of the Λ_b baryon (taken as $f_{\Lambda_b} = 4.28^{+0.75}_{-0.64} \times 10^{-3}\text{GeV}^2$) and the Λ_b baryon wave function shape parameter (taken as $\beta = 1.0 \pm 0.2$ GeV). The second error is the combined error from the hard scale t, defined in Eq. (49), which is varied from $0.75t$ to $1.25t$, and the renormalization scale of the Wilson coefficients, given in Table I. The third error is the combined uncertainty due to the CKM matrix elements.

We observe from Table VIII that the results for the conventional pQCD and the hybrid pQCD approaches do not differ very much, although in the hybrid approach the factorizable contributions have increased by almost an order of magnitude as compared to the conventional pQCD approach. The reason for this is that in the hybrid approach the factorizable amplitudes f_i are still only a fraction of the non-factorizable amplitudes, as is apparent by comparing the results in Table VII. Of course, it remains to be checked if the non-factorizable amplitude is correctly estimated in the pQCD approach for the b-baryonic decays due to the exchange of two gluons. This involves, among other diagrams, those where both the gluons are attached to the same outgoing quark line (see, for example, the diagrams in the fourth row in Fig. 4). These contributions are more sharply peaked, compared to the others encountered here or in the decays of B-mesons, which involve single gluon attachments on a quark line.

The ratio of the decay rates for the $\Lambda_b \to p\pi$ and $\Lambda_b \to pK$ decays, called below $R_{\pi K}(\Lambda_b)$, can

be calculated from Table VIII, and is estimated by us as

$$R_{\pi K}(\Lambda_b) \equiv \frac{BR(\Lambda_b \to p\pi)}{BR(\Lambda_b \to pK)} = 2.6^{+2.0}_{-0.5} \tag{64}$$

in the hybrid pQCD approach. This can be understood from Eqs. (56-57), which show that the QCD penguin operators contribute to the coefficients f_1 and f_2 (defined in Eq. (44)) in the combination $a_4 + R_1^K a_6$ and $a_4 - R_2^K a_6$, respectively. This is quite different from the two-body hadronic decays of the B mesons, $B \to PP$ or $B \to PV$, where $P(V)$ is a light pseudoscalar (vector) meson. The key point is that both the hadronic matrix elements $\langle \Lambda(P)|\bar{s}\gamma_\mu b|\Lambda_b(P+q)\rangle$ and $\langle \Lambda(P)|\bar{s}\gamma_\mu\gamma_5 b|\Lambda_b(P+q)\rangle$ contribute to the baryonic decays. Theoretical predictions presented here deviate from the experimental data $R_{\pi K}(\Lambda_b) = 0.66 \pm 0.14 \pm 0.08$ [24]. Whether this discrepancy reflects the inadequacy of the current theoretical formalism embedded in the standard model, or the standard model itself, or requires improved data remains to be seen. We note *en passant* that the estimates of the branching ratios for the decays $\Lambda_b \to p\pi$ and $\Lambda_b \to pK$, and hence of the quantity $R_{\pi K}(\Lambda_b)$, reported in [19] in the generalized factorization approximation, are in error due to the incorrect relative sign of the two terms in Eq. (18) in that paper. We are convinced that the correct relative sign in question is given in our Eq. (53).

As for the direct CP asymmetries, theoretical predictions suffer from large uncertainties due to the hadronic distributions, the hard scattering and the renormalization scales in the factorizable amplitudes. For the CP asymmetries, one needs the complete NNLO vertex corrections, as only with this input will it be possible to make quantitative predictions. As can be seen from Table VIII, theoretical estimates for the parameter α for the decay $\Lambda_b \to p\pi$ have negative values in both the pQCD approaches, reflecting the $(V-A)$ structure of the weak current [51]. It is pointed out in [52] that the parameter α in $B_i(\frac{1}{2}^+) \to B_f(\frac{1}{2}^+)P(V)$ decays approaches -1 in the soft pseudoscalar meson or vector meson limit, i.e., for $m_P \to 0$ or $m_V \to 0$. This argument, however, is only valid for the tree-dominated processes. As for the $\Lambda_b \to pK$ decay, the contributions from the QCD penguin operators are comparable to that of the tree amplitude. The operator O_6 contributes to the $\Lambda_b \to p$ transition via the $(V+A)$ current (see Eq. (53)) and the Wilson coefficient a_6 is very sensitive to the energy scale as can be seen from Table I. Hence, the asymmetry parameter α can flip its sign for the $\Lambda_b \to pK$ decay due to the large penguin contributions. As a final remark, we find that the predictions for the parameter α in the $\Lambda_b \to p\pi$ decay are relatively stable with respect to the variations of hadronic parameters, the CKM matrix elements and the hard scale, and therefore it serves as a good quantity to test the standard model [31].

IV. DISCUSSIONS AND CONCLUSIONS

Thanks to the current and impending experimental programs at the Tevatron and the LHC, dedicated studies of the decays of the Λ_b baryon (and other heavy baryons) will be carried out, following the first measurements of the decays $\Lambda_b \to p\pi,\ pK$, performed at the Tevatron. Baryonic decays are flavor self-tagging processes. Therefore, they should be easier to reconstruct experimentally. In particular, the CP-asymmetry measurements amount to counting these self-tagged decay modes and their CP-conjugates. From the theoretical viewpoint, however, b-baryon decays are less tractable as the underlying QCD dynamics is more involved. Hence, it is far from being obvious if the theoretical approaches developed for the quantitative studies of the two-body non-leptonic decays of the B-mesons will work also for the corresponding b-baryon decays. We have carried out an exploratory study of the charmless hadronic decays $\Lambda_b \to p\pi,\ pK$ in the pQCD approach and find that the factorizable diagrams in the conventional pQCD approach contribute very little to the branching ratios, as the hard (perturbative) contributions to the baryonic transition form factors in this case turn out to be quite small compared to the estimates dominated by the soft dynamics. As an alternative, we adopted a hybrid approach, in spirit similar to the one advocated in Ref. [49] for the analysis of the color-suppressed decays, such as $B^0 \to J/\psi K^0$. An essential characteristic of this hybrid scheme is that the transition form factors are treated as non-perturbative objects, i.e., they are input in the theoretical analysis and are not computed perturbatively, as in the conventional pQCD approach. Employing the form factors estimated in the LCSR approach, we find that the factorizable contributions are no longer negligible, though for the two decays worked out here, the amplitudes are still dominated by the non-factorizing contributions.

Our predictions for the branching fraction for the decay $\Lambda_b \to p\pi$, which is dominated by the tree diagrams, are essentially in agreement with the current data, whereas estimates of the branching ratio for the $\Lambda_b \to pK$ decay, dominated by the penguin-amplitude, are found to be smaller typically by a factor 2. This deserves an improved theoretical analysis, as the data gets consolidated. The asymmetry parameter α associated with the anisotropic angular distribution of the proton produced in the polarized Λ_b baryon decays is also derived and is found to be relatively stable with respect to variations of hadronic inputs and higher-order corrections in $\Lambda_b \to p\pi$ decay. The asymmetry parameter α in the $\Lambda_b \to pK$ decay, however, can flip its sign due to the large penguin contributions and the sensitive scale dependence of the effective Wilson coefficient $a_6(\mu)$. The Feynman diagrams (G) with the three-gluon-vertices present in the perturbative amplitudes included in this work are found to be less important compared with the T diagrams. However,

these three-gluon-vertex diagrams are comparable to the C diagrams, as can be seen from Table III, and hence they may induce significant corrections to the color suppressed modes, such as the $\Lambda_b \to \Lambda J/\psi$ decay. Finally, quantitative estimates of the CP asymmetries presented here show large scale uncertainties and require NNLO vertex corrections to be firmed up, which are not yet available completely.

Acknowledgments

This work is partly supported by the National Science Foundation of China under Grant No.10735080 and 10625525 and by the German Academic Exchange Program (DAAD). The authors would like to thank Hai-Yang Cheng, Hsiang-nan Li, Run-Hui Li and Yue-Long Shen for valuable comments. Y. M. W. would like to acknowledge Lei Dang, Cheng Li, Ping Ren, Qian Wang, Xiao-Xia Wang and Yu-Min Wang for allowing us to share the computing resources. H. Z. is grateful to Marco Drewes, Christian Hambrock, Sebastian Mendizabal, Satoshi Mishima and Alexander Parkhomenko for helpful discussions during his stay at DESY.

APPENDIX A: FOURIER INTEGRATIONS AND b-SPACE MEASURES

We list below the Fourier integration formulae which have been employed in the derivation of the hard amplitudes in the impact parameter (or b) space. The symbols J_1, N_1, K_0 and K_1 are the various Bessel functions; z_i are the Feynman parameters; and the relation

$$K_n(-iz) = \frac{\pi i}{2} e^{\frac{in\pi}{2}} [J_n(z) + iN_n(z)] \tag{A1}$$

has been used used in the derivation of the Fourier transformation. With this, we get:

$$\int d^2k \frac{e^{i\mathbf{k}\cdot\mathbf{b}}}{k^2+A} = 2\pi\{K_0(\sqrt{A}b)\theta(A) + \frac{\pi i}{2}[J_0(\sqrt{|A|}b) + iN_0(\sqrt{|A|}b)]\theta(-A)\}, \tag{A2}$$

$$\int d^2k \frac{e^{i\mathbf{k}\cdot\mathbf{b}}}{(k^2+A)(k^2+B)} = \pi \int_0^1 dz \frac{b}{\sqrt{|Z_1|}}\{K_1(\sqrt{Z_1}b)\theta(Z_1) + \frac{\pi}{2}[N_1(\sqrt{|Z_1|}b) - iJ_1(\sqrt{|Z_1|}b)]\theta(-Z_1)\}, \tag{A3}$$

$$\begin{aligned}
&\int d^2k_1 d^2k_2 \frac{e^{i(\mathbf{k}_1\cdot\mathbf{b}_1+\mathbf{k}_2\cdot\mathbf{b}_2)}}{(k_1^2+A)(k_2^2+B)[(k_1+k_2)^2+C]} \\
&= \pi^2 \int_0^1 \frac{dz_1 dz_2}{z_1(1-z_1)} \frac{\sqrt{X_2}}{\sqrt{|Z_2|}} \left\{ K_1(\sqrt{X_2 Z_2})\theta(Z_2) + \frac{\pi}{2}\left[N_1(\sqrt{X_2|Z_2|}) - iJ_1(\sqrt{X_2|Z_2|})\right]\theta(-Z_2) \right\}, \\
&\quad \text{where } A > 0\ , \text{ and } B, C \text{ are arbitrary}\ ,
\end{aligned} \tag{A4}$$

$$\int d^2k_1 d^2k_2 d^2k_3 \frac{e^{i(\mathbf{k}_1\cdot\mathbf{b}_1+\mathbf{k}_2\cdot\mathbf{b}_2+\mathbf{k}_3\cdot\mathbf{b}_3)}}{(k_1^2+A)(k_2^2+B)(k_3^2+C)[(k_1+k_2+k_3)^2+D]}$$
$$= \pi^3 \int_0^1 \frac{dz_1 dz_2 dz_3}{z_1(1-z_1)z_2(1-z_2)} \frac{\sqrt{X_3}}{\sqrt{|Z_3|}} \left\{ K_1(\sqrt{X_3 Z_3})\theta(Z_3) + \frac{\pi}{2}\left[N_1(\sqrt{X_3|Z_3|}) - iJ_1(\sqrt{X_3|Z_3|})\right]\theta(-Z_3)\right\},$$
$$A, B > 0 \text{ , and } C, D \text{ arbitrary ,} \tag{A5}$$

with the variables,

$$Z_1 = A\,z + B\,(1-z)\,, \tag{A6}$$
$$Z_2 = A\,(1-z_2) + \frac{z_2}{z_1(1-z_1)}[B\,(1-z_1) + C\,z_1]\,,$$
$$X_2 = (b_1 - z_1 b_2)^2 + \frac{z_1(1-z_1)}{z_2} b_2^2\,, \tag{A7}$$
$$Z_3 = A\,(1-z_3) + \frac{z_3}{z_2(1-z_2)}\left\{ B\,(1-z_2) + \frac{z_2}{z_1(1-z_1)}[C\,(1-z_1) + D\,z_1]\right\}\,,$$
$$X_3 = [b_1 - b_2 z_2 - b_3 z_1(1-z_2)]^2 + \frac{z_2(1-z_2)}{z_3}(b_2 - b_3 z_1)^2 + \frac{z_1(1-z_1)z_2(1-z_2)}{z_2 z_3} b_3^2\,. \tag{A8}$$

APPENDIX B: FACTORIZATION FORMULAE FOR THE FEYNMAN DIAGRAMS WITH VARIOUS TOPOLOGIES

In this appendix, we would like to collect the factorizable formulae for typical diagrams corresponding to different topologies in the $\Lambda_b \to p\pi$ decays. In doing so, we give the expressions only for a certain representative set of diagrams in each class, with the rest following from appropriate substitutions.

1. Factorization formulae for the color allowed emission diagrams

For the first diagram in Fig. 4 (labeled as figure T_1), which is a factorizable diagram and included only in the conventional pQCD approach, we have:

$$f_1^{T_1} = G_F \frac{\pi^2}{18\sqrt{3}} f_{\Lambda_b} f_p \int [dx] \int [dx'] \int dy\, [\alpha_s(t^{T_1})]^2 \psi_{\Lambda_b}(x)$$
$$\times \left\{ \left[16 M_{\Lambda_b}^5 [(\frac{1}{3}C_1 + C_2)V_{ub}V_{ud}^* + (\frac{1}{3}C_3 + C_4 + \frac{1}{3}C_9 + C_{10})V_{tb}V_{td}^*](-2x_2 + (1-2x_2)x_1' - x_3')\phi_M^A(y) \right.\right.$$
$$\left. -32 m_0 M_{\Lambda_b}^4 (\frac{1}{3}C_5 + C_6 + \frac{1}{3}C_7 + C_8)V_{tb}V_{td}^*(4x_1 + 4x_3 - x_3' - 3)\phi_M^P(y)\right] \psi_p^V(x')$$
$$+ \left[16 M_{\Lambda_b}^5 [(\frac{1}{3}C_1 + C_2)V_{ub}V_{ud}^* + (\frac{1}{3}C_3 + C_4 + \frac{1}{3}C_9 + C_{10})V_{tb}V_{td}^*](1 + x_2')\phi_M^A(y) \right.$$
$$\left. -32 m_0 M_{\Lambda_b}^4 (\frac{1}{3}C_5 + C_6 + \frac{1}{3}C_7 + C_8)V_{tb}V_{td}^*(x_3' - 1)\phi_M^P(y)\right] \psi_p^A(x')$$

$$
\begin{aligned}
&+\Big[16M_{\Lambda_b}^5[(\frac{1}{3}C_1+C_2)V_{ub}V_{ud}^*+(\frac{1}{3}C_3+C_4+\frac{1}{3}C_9+C_{10})V_{tb}V_{td}^*](2(x_1+x_3))\phi_M^A(y)\\
&\quad+32m_0M_{\Lambda_b}^4(\frac{1}{3}C_5+C_6+\frac{1}{3}C_7+C_8)V_{tb}V_{td}^*(2(x_1+x_3))\phi_M^T(y)\Big]\psi_p^T(x')\Big\}\\
\times\ &\frac{1}{16\pi^2}\int b_1'db_1'\int b_2db_2\int b_3db_3\int d\theta_1\int d\theta_2\exp[-S^{T_1}(x,x',b,b')]\,K_0(\sqrt{D^{T_1}}|b_3|)\\
&\int_0^1\frac{dz_1dz_2}{z_1(1-z_1)}\sqrt{\frac{X_2^{T_1}}{|Z_2^{T_1}|}}\Big\{K_1(\sqrt{X_2^{T_1}Z_2^{T_1}})\Theta(Z_2^{T_1})+\frac{\pi}{2}[J_1(\sqrt{X_2^{T_1}|Z_2^{T_1}|})+iN_1(\sqrt{X_2^{T_1}|Z_2^{T_1}|})]\Theta(-Z_2^{T_1})\Big\},
\end{aligned}
\tag{B1}
$$

where the auxiliary functions in the above expression are defined as

$$
\begin{aligned}
&A^{T_1}=(1-x_1')M_{\Lambda_b}^2,B^{T_1}=(x_2+x_3'-x_2x_3')M_{\Lambda_b}^2,C^{T_1}=x_2x_2'M_{\Lambda_b}^2,\ D^{T_1}=x_3x_3'M_{\Lambda_b}^2,\\
&Z_2^{T_1}=A^{T_1}(1-z_2)+\frac{z_2}{z_1(1-z_1)}[B^{T_1}(1-z_1)+C^{T_1}z_1],\\
&X_2^{T_1}=(b_1'-z_1b_2)^2+\frac{z_1(1-z_1)}{z_2}b_2^2.\\
&t^{T_1}=max(\sqrt{|A^{T_1}|},\sqrt{|B^{T_1}|},\sqrt{|C^{T_1}|},\sqrt{|D^{T_1}|},\omega,\omega').
\end{aligned}
\tag{B2}
$$

Similarly, the factorization formula for the form factor f_2 contributed by T_1 can be written as

$$
\begin{aligned}
f_2^{T_1}\ =\ &G_F\frac{\pi^2}{18\sqrt{3}}f_{\Lambda_b}f_p\int[dx]\int[dx']\int dy\,[\alpha_s(t^{T_1})]^2\psi_{\Lambda_b}(x)\\
\times\ &\Big\{\Big[16M_{\Lambda_b}^5[(\frac{1}{3}C_1+C_2)V_{ub}V_{ud}^*+(\frac{1}{3}C_3+C_4+\frac{1}{3}C_9+C_{10})V_{tb}V_{td}^*](1+x_2')\phi_M^A(y)\\
&\quad+32m_0M_{\Lambda_b}^4(\frac{1}{3}C_5+C_6+\frac{1}{3}C_7+C_8)V_{tb}V_{td}^*(x_3'-1)\phi_M^P(y)\Big]\psi_p^V(x')\\
&+\Big[16M_{\Lambda_b}^5[(\frac{1}{3}C_1+C_2)V_{ub}V_{ud}^*+(\frac{1}{3}C_3+C_4+\frac{1}{3}C_9+C_{10})V_{tb}V_{td}^*](-2x_2+(1-2x_2)x_1'-x_3')\phi_M^A(y)\\
&\quad-32m_0M_{\Lambda_b}^4(\frac{1}{3}C_5+C_6+\frac{1}{3}C_7+C_8)V_{tb}V_{td}^*(4x_1+4x_3-x_3'-3)\phi_M^P(y)\Big]\psi_p^A(x')\\
&+\Big[16M_{\Lambda_b}^5[(\frac{1}{3}C_1+C_2)V_{ub}V_{ud}^*+(\frac{1}{3}C_3+C_4+\frac{1}{3}C_9+C_{10})V_{tb}V_{td}^*](2(x_1+x_3))\phi_M^A(y)\\
&\quad-32m_0M_{\Lambda_b}^4(\frac{1}{3}C_5+C_6+\frac{1}{3}C_7+C_8)V_{tb}V_{td}^*(2(x_1+x_3))\phi_M^T(y)\Big]\psi_p^T(x')\Big\}\\
\times\ &\frac{1}{16\pi^2}\int b_1'db_1'\int b_2db_2\int b_3db_3\int d\theta_1\int d\theta_2\exp[-S^{T_1}(x,x',b,b')]\,K_0(\sqrt{D^{T_1}}|b_3|)\\
&\int_0^1\frac{dz_1dz_2}{z_1(1-z_1)}\sqrt{\frac{X_2^{T_1}}{|Z_2^{T_1}|}}\Big\{K_1(\sqrt{X_2^{T_1}Z_2^{T_1}})\Theta(Z_2^{T_1})+\frac{\pi}{2}[J_1(\sqrt{X_2^{T_1}|Z_2^{T_1}|})+iN_1(\sqrt{X_2^{T_1}|Z_2^{T_1}|})]\Theta(-Z_2^{T_1})\Big\}.
\end{aligned}
\tag{B3}
$$

For the 25th diagram in Fig. 4 (labeled as T_{25}), which is a non-factorizable diagram, we have:

$$
f_1^{T_{25}}\ =\ G_F\frac{\pi^2}{144\sqrt{3}}f_{\Lambda_b}f_p\int[dx]\int[dx']\int dy\,[\alpha_s(t^{T_{25}})]^2\psi_{\Lambda_b}(x)
$$

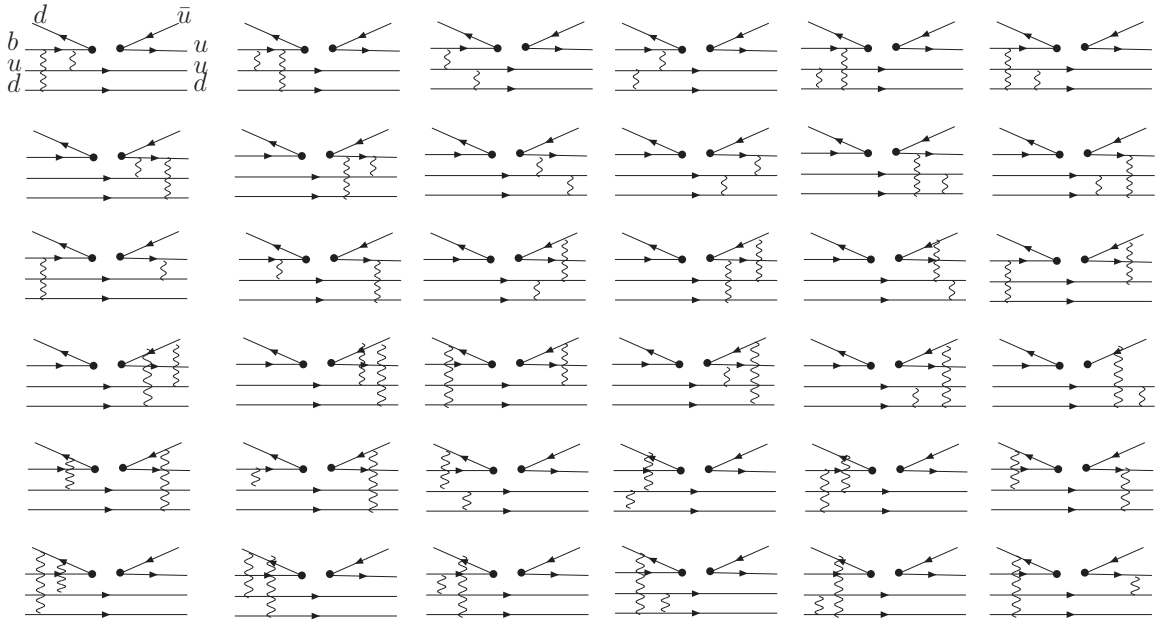

FIG. 4: External W emission (T) diagrams for the $\Lambda_b \to p\pi$ decay to the lowest order in the pQCD approach where the dots denote the weak interactions vertices. The two hard gluons are needed to transfer the large momentum to the light quarks in the initial state so that these two light quarks are collinear in the final state. These diagrams are called $T_1, T_2, ..., T_{36}$ in the text.

$$
\begin{aligned}
\times\ & \Bigg\{\Bigg[16M_{\Lambda_b}^5[(\frac{8}{3}C_1-2C_2)V_{ub}V_{ud}^*+(\frac{8}{3}C_3-2C_4+\frac{8}{3}C_9-2C_{10})V_{tb}V_{td}^*](x_2-y)(-x_3+x_3'-y+1)\phi_M^A(y)\\
&\quad +16m_0M_{\Lambda_b}^4(\frac{8}{3}C_5-2C_6+\frac{8}{3}C_7-2C_8)V_{tb}V_{td}^*x_2'(1-x_3-y)(\phi_M^P(y)-\phi_M^T(y))\Bigg]\psi_p^V(x')\\
&+\Bigg[16M_{\Lambda_b}^5[(\frac{8}{3}C_1-2C_2)V_{ub}V_{ud}^*+(\frac{8}{3}C_3-2C_4+\frac{8}{3}C_9-2C_{10})V_{tb}V_{td}^*](x_2-y)(1-x_3-x_3'-y)\phi_M^A(y)\\
&\quad +16m_0M_{\Lambda_b}^4(\frac{8}{3}C_5-2C_6+\frac{8}{3}C_7-2C_8)V_{tb}V_{td}^*x_2'(1-x_3-y)(\phi_M^P(y)-\phi_M^T(y))\Bigg]\psi_p^A(x')\\
&+\Bigg[32M_{\Lambda_b}^5[(\frac{8}{3}C_1-2C_2)V_{ub}V_{ud}^*+(\frac{8}{3}C_3-2C_4+\frac{8}{3}C_9-2C_{10})V_{tb}V_{td}^*](x_2-y)(1-x_3-y)\phi_M^A(y)\\
&\quad +32m_0M_{\Lambda_b}^4(\frac{8}{3}C_5-2C_6+\frac{8}{3}C_7-2C_8)V_{tb}V_{td}^*x_3'(y-x_2)\phi_M^T(y)\Bigg]\psi_p^T(x')\Bigg\}\\
\times\ & \frac{1}{32\pi^2}\int b_2db_2\int b_3db_3\int b_qdb_q\int d\theta_1\int d\theta_2\exp[-S^{T_{25}}(x,x',y,b,b',b_q)]\int_0^1\frac{dz_1dz_2dz_3}{z_1(1-z_1)z_2(1-z_2)}\\
&\sqrt{\frac{X_3^{T_{25}}}{|Z_3^{T_{25}}|}}\Bigg\{K_1(\sqrt{X_3^{T_{25}}Z_3^{T_{25}}})\Theta(Z_3^{T_{25}})+\frac{\pi}{2}[J_1(\sqrt{X_3^{T_{25}}|Z_3^{T_{25}}|})+iN_1(\sqrt{X_3^{T_{25}}|Z_3^{T_{25}}|})]\Theta(-Z_3^{T_{25}})\Bigg\},
\end{aligned}
\tag{B4}
$$

where the auxiliary functions in the expressions above are defined as

$$
\begin{aligned}
&A^{T_{25}}=x_3'(x_3+y-1)M_{\Lambda_b}^2, B^{T_{25}}=x_2'(x_2-y)M_{\Lambda_b}^2, C^{T_{25}}=x_2x_2'M_{\Lambda_b}^2,\ D^{T_{25}}=x_3x_3'M_{\Lambda_b}^2\\
&X_3^{T_{25}}=(b_2-(b_3-b_q)z_2+b_qz_1(1-z_2))^2+\frac{z_2(1-z_2)}{z_3}(b_3-b_q+b_qz_1)^2+\frac{z_1(1-z_1)z_2(1-z_2)}{z_2z_3}b_q^2\ ,
\end{aligned}
$$

$$Z_3^{T_{25}} = C(1-z_3) + \frac{z_3}{z_2(1-z_2)}[D(1-z_2) + \frac{z_2}{z_1(1-z_1)}[A(1-z_1)+Bz_1]],$$
$$t^{T_{25}} = max(\sqrt{|A^{T_{25}}|}, \sqrt{|B^{T_{25}}|}, \sqrt{|C^{T_{25}}|}, \sqrt{|D^{T_{25}}|}, \omega, \omega', \omega_q). \tag{B5}$$

Similarly, the factorization formula for the form factor f_2 contributed by T_{25} can be written as

$$\begin{aligned}
f_2^{T_{25}} &= G_F \frac{\pi^2}{144\sqrt{3}} f_{\Lambda_b} f_p \int [dx] \int [dx'] \int dy\, [\alpha_s(t^{T_{25}})]^2 \psi_{\Lambda_b}(x) \\
&\times \Big\{ \Big[16 M_{\Lambda_b}^5 [(\frac{8}{3}C_1 - 2C_2) V_{ub}V_{ud}^* + (\frac{8}{3}C_3 - 2C_4 + \frac{8}{3}C_9 - 2C_{10}) V_{tb}V_{td}^*](x_2 - y)(1 - x_3 - x_3' - y)\phi_M^A(y) \\
&\quad -16 m_0 M_{\Lambda_b}^4 (\frac{8}{3}C_5 - 2C_6 + \frac{8}{3}C_7 - 2C_8) V_{tb}V_{td}^* x_2' (1 - x_3 - y)(\phi_M^P(y) - \phi_M^T(y)) \Big] \psi_p^V(x') \\
&\quad + \Big[16 M_{\Lambda_b}^5 [(\frac{8}{3}C_1 - 2C_2) V_{ub}V_{ud}^* + (\frac{8}{3}C_3 - 2C_4 + \frac{8}{3}C_9 - 2C_{10}) V_{tb}V_{td}^*](x_2 - y)(-x_3 + x_3' - y + 1)\phi_M^A(y) \\
&\quad -16 m_0 M_{\Lambda_b}^4 (\frac{8}{3}C_5 - 2C_6 + \frac{8}{3}C_7 - 2C_8) V_{tb}V_{td}^* x_2' (1 - x_3 - y)(\phi_M^P(y) - \phi_M^T(y)) \Big] \psi_p^A(x') \\
&\quad + \Big[32 M_{\Lambda_b}^5 [(\frac{8}{3}C_1 - 2C_2) V_{ub}V_{ud}^* + (\frac{8}{3}C_3 - 2C_4 + \frac{8}{3}C_9 - 2C_{10}) V_{tb}V_{td}^*](x_2 - y)(1 - x_3 - y)\phi_M^A(y) \\
&\quad -32 m_0 M_{\Lambda_b}^4 (\frac{8}{3}C_5 - 2C_6 + \frac{8}{3}C_7 - 2C_8) V_{tb}V_{td}^* x_3' (y - x_2)\phi_M^T(y) \Big] \psi_p^T(x') \Big\} \\
&\times \frac{1}{32\pi^2} \int b_2 db_2 \int b_3 db_3 \int b_q db_q \int d\theta_1 \int d\theta_2 \exp[-S^{T_{25}}(x, x', y, b, b', b_q)] \int_0^1 \frac{dz_1 dz_2 dz_3}{z_1(1-z_1)z_2(1-z_2)} \\
&\sqrt{\frac{X_3^{T_{25}}}{|Z_3^{T_{25}}|}} \Big\{ K_1(\sqrt{X_3^{T_{25}} Z_3^{T_{25}}}) \Theta(Z_3^{T_{25}}) + \frac{\pi}{2}[J_1(\sqrt{X_3^{T_{25}}|Z_3^{T_{25}}|}) + iN_1(\sqrt{X_3^{T_{25}}|Z_3^{T_{25}}|})] \Theta(-Z_3^{T_{25}}) \Big\}.
\end{aligned} \tag{B6}$$

As can be seen from Eq. (B5), the color structures for the baryonic decays are quite different from that in the mesonic decays. Only the operators with the color indices the same as O_1 can contribute to the non-factorizable emission diagrams in the two-body hadronic B meson decays. However, all the operators $O_i (i = 1 - 10)$ contribute to the non-factorizable emission diagrams in the non-leptonic two-body bottom baryon Λ_b decays. In particular, the $(V-A)\otimes(V+A)$ type operators have no effect on the non-factorizable emission diagrams for the hadronic $B \to PP$ decays, if the emitted meson is a π, η or η'. In contrast, both the $(V-A)\otimes(V-A)$ and $(V-A)\otimes(V+A)$ operators contribute to the non-factorizable emission diagrams in their baryonic counterparts.

2. Factorization formulae for the color suppressed emission diagrams

For the first diagram in Fig. 5 (labeled as C_1), a factorizable diagram, we have:

$$\begin{aligned}
f_1^{C_1} &= G_F \frac{\pi^2}{54\sqrt{3}} f_{\Lambda_b} f_p \int [dx] \int [dx'] \int dy\, [\alpha_s(t^{C_1})]^2 \psi_{\Lambda_b}(x) \\
&\times \Big\{ \Big[-16 M_{\Lambda_b}^4 (-(C_5 + C_7) + (C_6 + C_8)) V_{tb}V_{td}^* [m_0 (x_2(y-2) + (y-1)y)(\phi_M^P(y) + \phi_M^T(y))
\end{aligned}$$

$$
\begin{aligned}
&-M_{\Lambda_b}(x_2(y-1)+(y-2)y)\phi_M^A(y)\,]\Big](\psi_p^V(x')-\psi_p^A(x'))\\
&+\Big[-32M_{\Lambda_b}^4(-(C_5+C_7)+(C_6+C_8))V_{tb}V_{td}^*\,(y-1)\,[m_0(x_2+y-1)(\phi_M^P(y)+\phi_M^T(y))\\
&-M_{\Lambda_b}\phi_M^A(y)\,]\Big]\psi_p^T(x')\Big\}\\
\times\;&\frac{1}{16\pi^2}\int b_2db_2\int b_2'db_2'\int b_qdb_q\int d\theta_1\int d\theta_2\exp[-S^{C_1}(x,x',b,b')]\,K_0(\sqrt{D^{C_1}}|b_2+b_2'-b_q|)\\
&\int_0^1\frac{dz_1dz_2}{z_1(1-z_1)}\sqrt{\frac{X_2^{C_1}}{|Z_2^{C_1}|}}\Big\{K_1(\sqrt{X_2^{C_1}Z_2^{C_1}})\Theta(Z_2^{C_1})+\frac{\pi}{2}[J_1(\sqrt{X_2^{C_1}|Z_2^{C_1}|})+iN_1(\sqrt{X_2^{C_1}|Z_2^{C_1}|})]\Theta(-Z_2^{C_1})\Big\},
\end{aligned}
\tag{B7}
$$

where the auxiliary functions in the expressions above are defined as

$$
\begin{aligned}
&A^{T_1}=(x_2'+y-x_2'y)M_{\Lambda_b}^2, B^{T_1}=(x_2+y)M_{\Lambda_b}^2, C^{T_1}=x_2x_2'M_{\Lambda_b}^2,\;D^{T_1}=x_3yM_{\Lambda_b}^2,\\
&Z_2^{T_1}=A^{T_1}(1-z_2)+\frac{z_2}{z_1(1-z_1)}[B^{T_1}(1-z_1)+C^{T_1}z_1],\\
&X_2^{T_1}=(b_1'+z_1b_2)^2+\frac{z_1(1-z_1)}{z_2}b_2^2,\\
&t^{C_1}=max(\sqrt{|A^{C_1}|},\sqrt{|B^{C_1}|},\sqrt{|C^{C_1}|},\sqrt{|D^{C_1}|},\omega,\omega').
\end{aligned}
\tag{B8}
$$

Similarly, the factorization formula for the form factor f_2 contributed by C_1 can be written as

$$
\begin{aligned}
f_2^{C_1}\;=\;&G_F\frac{\pi^2}{54\sqrt{3}}f_{\Lambda_b}f_p\int[dx]\int[dx']\int dy\,[\alpha_s(t^{C_1})]^2\psi_{\Lambda_b}(x)\\
\times\;&\Big\{\Big[-16M_{\Lambda_b}^4(-(C_5+C_7)+(C_6+C_8))V_{tb}V_{td}^*\,[m_0(x_2(y-2)+(y-1)y)(\phi_M^P(y)+\phi_M^T(y))\\
&-M_{\Lambda_b}(x_2(y-1)+(y-2)y)\phi_M^A(y)\,]\Big](\psi_p^V(x')-\psi_p^A(x'))\\
&+\Big[32M_{\Lambda_b}^4(-(C_5+C_7)+(C_6+C_8))V_{tb}V_{td}^*\,(y-1)\,[m_0(x_2+y-1)(\phi_M^P(y)+\phi_M^T(y))\\
&-M_{\Lambda_b}\phi_M^A(y)\,]\Big]\psi_p^T(x')\Big\}\\
\times\;&\frac{1}{16\pi^2}\int b_2db_2\int b_2'db_2'\int b_qdb_q\int d\theta_1\int d\theta_2\exp[-S^{C_1}(x,x',b,b')]\,K_0(\sqrt{D^{C_1}}|b_2+b_2'-b_q|)\\
&\int_0^1\frac{dz_1dz_2}{z_1(1-z_1)}\sqrt{\frac{X_2^{C_1}}{|Z_2^{C_1}|}}\Big\{K_1(\sqrt{X_2^{C_1}Z_2^{C_1}})\Theta(Z_2^{C_1})+\frac{\pi}{2}[J_1(\sqrt{X_2^{C_1}|Z_2^{C_1}|})+iN_1(\sqrt{X_2^{C_1}|Z_2^{C_1}|})]\Theta(-Z_2^{C_1})\Big\}.
\end{aligned}
\tag{B9}
$$

For the 20th diagram in Fig. 5 (labeled C_{20}), a non-factorizable diagram, we have:

$$
\begin{aligned}
f_1^{C_{20}}\;=\;&G_F\frac{\pi^2}{27\sqrt{3}}f_{\Lambda_b}f_p\int[dx]\int[dx']\int dy\,[\alpha_s(t^{C_{20}})]^2\psi_{\Lambda_b}(x)\\
\times\;&\Big\{-32M_{\Lambda_b}^4((C_5+C_7)-(C_6+C_8))V_{tb}V_{td}^*\,[M_{\Lambda_b}x_3\phi_M^A(y)-2m_0(x_3-1)\phi_M^P(y)\,]\psi_p^T(x')\Big\}
\end{aligned}
$$

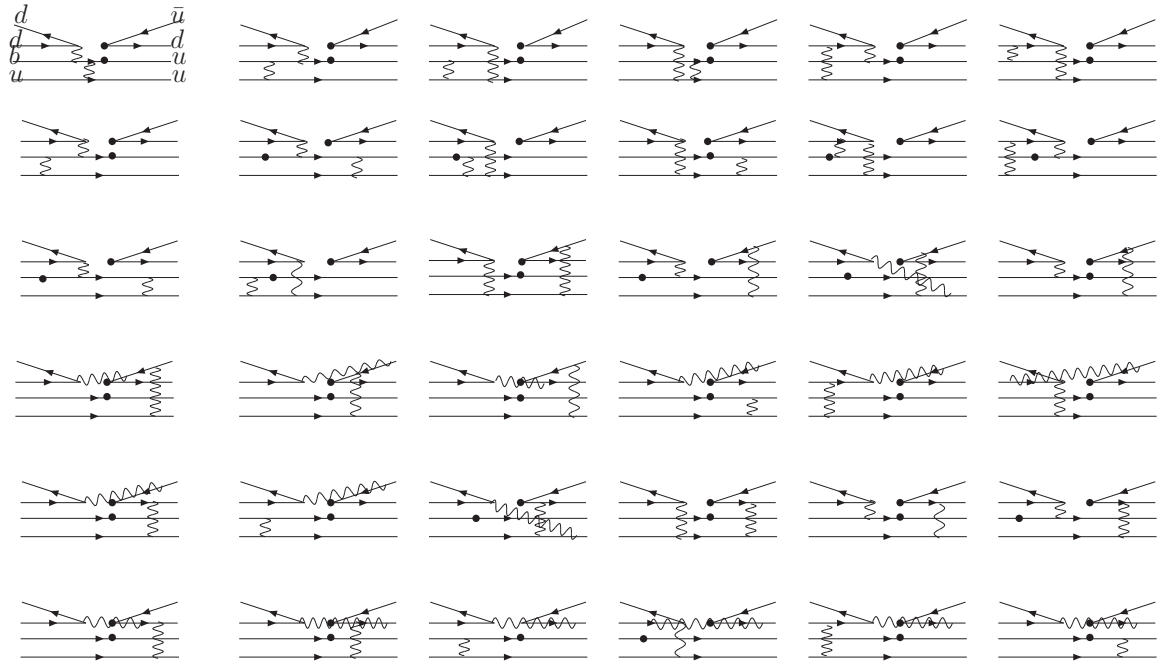

FIG. 5: Internal W emission (C) diagrams for the $\Lambda_b \to p\pi$ decay to lowest order in the PQCD approach where the dots denote the weak interactions vertices. As in the preceding figure, the two hard gluons are essential to transfer the large momentum to the light quarks in the initial state. These diagrams are called $C_1, C_2, ..., C_{36}$.

$$\times \frac{1}{16\pi^2}\int b_1 db_1 \int b_3 db_3 \int b_q db_q \int d\theta_1 \int d\theta_2 \exp[-S^{C_{20}}(x,x',y,b,b',b_q)]\, K_0(\sqrt{D^{C_{20}}}|b_2+b_2'-b_q|)$$
$$\int_0^1 \frac{dz_1 dz_2}{z_1(1-z_1)}\sqrt{\frac{X_2^{C_{20}}}{|Z_2^{C_{20}}|}}\Big\{K_1(\sqrt{X_2^{C_{20}}Z_2^{C_{20}}})\Theta(Z_2^{C_{20}}) + \frac{\pi}{2}[J_1(\sqrt{X_2^{C_{20}}|Z_2^{C_{20}}|}) + iN_1(\sqrt{X_2^{C_{20}}|Z_2^{C_{20}}|})]\Theta(-Z_2^{C_{20}})\Big\}, \tag{B10}$$

where the auxiliary functions in the above expression are defined as

$$\begin{aligned}
&A^{C_{20}} = x_3 M_{\Lambda_b}^2, B^{C_{20}} = -x_2' M_{\Lambda_b}^2, C^{C_{20}} = x_2 x_2' M_{\Lambda_b}^2,\ D^{C_{20}} = x_3 y M_{\Lambda_b}^2,\\
&Z_2^{C_{20}} = A^{C_{20}}(1-z_2) + \frac{z_2}{z_1(1-z_1)}[B^{C_{20}}(1-z_1) + C^{C_{20}} z_1],\\
&X_2^{C_{20}} = [(b_3+b_q) - z_1 b_1]^2 + \frac{z_1(1-z_1)}{z_2} b_1^2,\\
&t^{C_{20}} = max(\sqrt{|A^{C_{20}}|}, \sqrt{|B^{C_{20}}|}, \sqrt{|C^{C_{20}}|}, \sqrt{|D^{C_{20}}|}, \omega, \omega', \omega_q).
\end{aligned} \tag{B11}$$

Similarly, the factorization formula for the form factor f_2 contributed by C_{20} can be written as

$$f_1^{C_{20}} = -f_2^{C_{20}}. \tag{B12}$$

3. Factorization formulae for the exchange diagrams

For the 18th diagram in Fig. 6 (labeled as E_{18}), we have:

$$
\begin{aligned}
f_1^{E_{18}} &= G_F\frac{\pi^2}{54\sqrt{3}}f_{\Lambda_b}f_p\int[dx]\int[dx']\int dy\,[\alpha_s(t^{E_{18}})]^2\psi_{\Lambda_b}(x)\\
&\times\ \Big\{\Big[16m_0M_{\Lambda_b}^4[(C_1-C_2)V_{ub}V_{ud}^*+((C_3+C_9)-(C_4+C_{10}))V_{tb}V_{td}^*](y-1)(\phi_M^P(y)+\phi_M^T(y))\\
&\quad+16m_0M_{\Lambda_b}^4((C_5+C_7)-(C_6+C_8))V_{tb}V_{td}^*(y-1)(\phi_M^P(y)+\phi_M^T(y))\Big]\psi_p^V(x')\\
&\quad+\Big[16m_0M_{\Lambda_b}^4[(C_1-C_2)V_{ub}V_{ud}^*+((C_3+C_9)-(C_4+C_{10}))V_{tb}V_{td}^*](y-1)(\phi_M^P(y)+\phi_M^T(y))\\
&\quad-16m_0M_{\Lambda_b}^4((C_5+C_7)-(C_6+C_8))V_{tb}V_{td}^*(y-1)(\phi_M^P(y)+\phi_M^T(y))\Big]\psi_p^A(x')\Big\}\\
&\times\ \frac{1}{16\pi^2}\int b_2db_2\int b_3db_3\int b_qdb_q\int d\theta_1\int d\theta_2\exp[-S^{E_{18}}(x,x',y,b,b',b_q)]\\
&\quad\{K_0(\sqrt{C^{E_{18}}}|b_2'|)\theta(C^{E_{18}})+\frac{\pi i}{2}[J_0(\sqrt{|C^{E_{18}}|}|b_2'|)+iN_0(\sqrt{|C^{E_{18}}|}|b_2'|)]\theta(-C^{E_{18}})\}\int_0^1\frac{dz_1dz_2}{z_1(1-z_1)}\\
&\quad\sqrt{\frac{X_2^{E_{18}}}{|Z_2^{E_{18}}|}}\Big\{K_1(\sqrt{X_2^{E_{18}}Z_2^{E_{18}}})\Theta(Z_2^{E_{18}})+\frac{\pi}{2}[J_1(\sqrt{X_2^{E_{18}}|Z_2^{E_{18}}|})+iN_1(\sqrt{X_2^{E_{18}}|Z_2^{E_{18}}|})]\Theta(-Z_2^{E_{18}})\Big\},
\end{aligned}
\tag{B13}
$$

where the auxiliary functions in the expression above are defined as

$$
\begin{aligned}
&A^{E_{18}}=(x_3'-1)M_{\Lambda_b}^2, B^{E_{18}}=(y-1)(1-x_3')M_{\Lambda_b}^2, C^{E_{18}}=x_2'(y-1)M_{\Lambda_b}^2,\ D^{E_{18}}=x_3yM_{\Lambda_b}^2,\\
&Z_2^{E_{18}}=A^{E_{18}}(1-z_2)+\frac{z_2}{z_1(1-z_1)}[B^{E_{18}}(1-z_1)+D^{E_{18}}z_1],\\
&X_2^{E_{18}}=[b_3+z_1(b_2'+b_q)]^2+\frac{z_1(1-z_1)}{z_2}(b_2'+b_q)^2,\\
&t^{E_{18}}=max(\sqrt{|A^{E_{18}}|},\sqrt{|B^{E_{18}}|},\sqrt{|C^{E_{18}}|},\sqrt{|D^{E_{18}}|},\omega,\omega',\omega_q).
\end{aligned}
\tag{B14}
$$

Similarly, the factorization formula for the form factor f_2 contributed from E_{18} can be written as

$$
f_2^{E_{18}} = f_1^{E_{18}}. \tag{B15}
$$

For the 26th diagram in Fig. 6 (labeled as E_{26}), we have:

$$
\begin{aligned}
f_1^{E_{26}} &= G_F\frac{\pi^2}{54\sqrt{3}}f_{\Lambda_b}f_p\int[dx]\int[dx']\int dy\,[\alpha_s(t^{E_{26}})]^2\psi_{\Lambda_b}(x)\\
&\times\ \Big\{\Big[16m_0M_{\Lambda_b}^4[(C_1-C_2)V_{ub}V_{ud}^*+((C_3+C_9)-(C_4+C_{10}))V_{tb}V_{td}^*](1-y)(\phi_M^P(y)+\phi_M^T(y))\Big]\psi_p^V(x')\\
&\quad+\Big[16m_0M_{\Lambda_b}^4[(C_1-C_2)V_{ub}V_{ud}^*+((C_3+C_9)-(C_4+C_{10}))V_{tb}V_{td}^*](1-y)(\phi_M^P(y)+\phi_M^T(y))\Big]\psi_p^A(x')\\
&\quad+\Big[32M_{\Lambda_b}^4((C_5+C_7)-(C_6+C_8))V_{tb}V_{td}^*(y-1)[M_{\Lambda_b}(x_1'-1)\phi_M^A(y)
\end{aligned}
$$

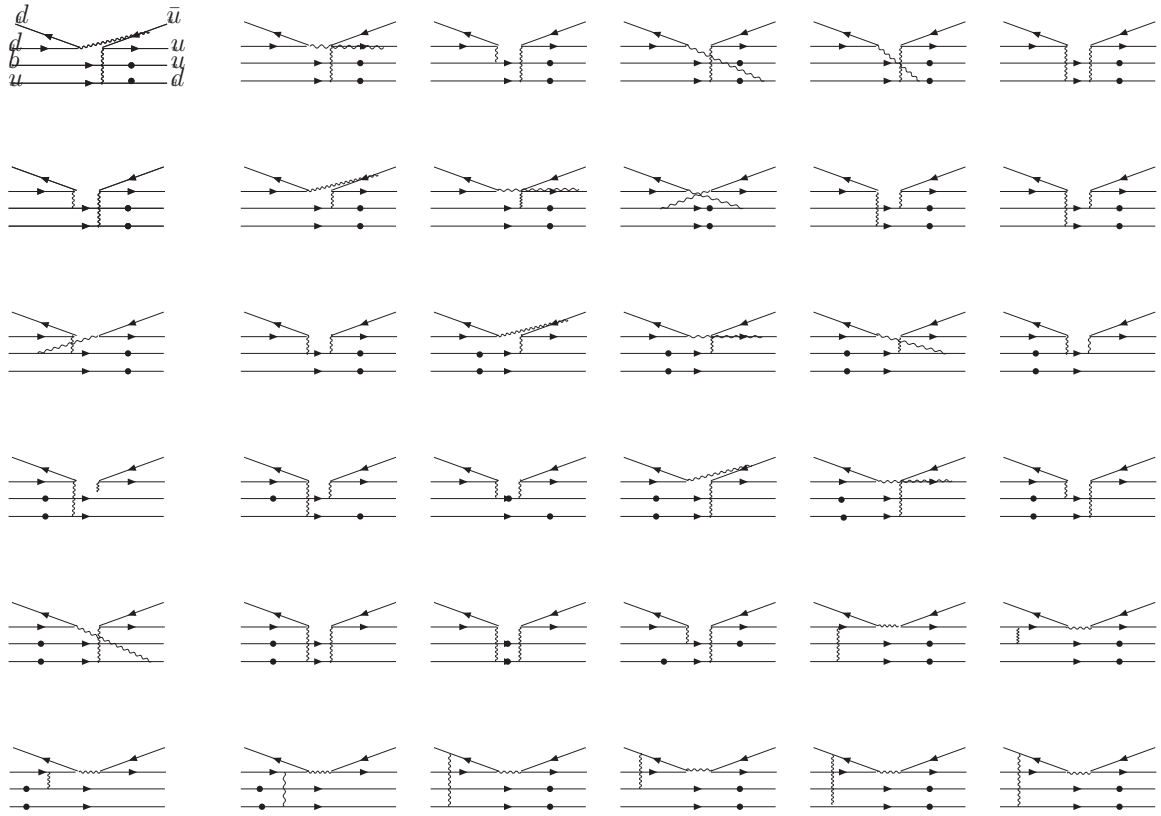

FIG. 6: W exchange (E) diagrams for the $\Lambda_b \to p\pi$ decay to lowest order in the pQCD approach where the dots denote the weak interactions vertices. As in the preceding figure, the two hard gluons are needed to transfer the large momentum to the light quarks in the initial state. These diarams are called $E_1, E_2, ..., E_{36}$.

$$
\begin{aligned}
&-m_0(x_1'-2)(\phi_M^P(y)+\phi_M^T(y))\Big]\psi_p^T(x')\Big\} \\
\times\ &\frac{1}{16\pi^2}\int b_1'db_1'\int b_2'db_2'\int b_q db_q\int d\theta_1\int d\theta_2\exp[-S^{E_{26}}(x,x',y,b,b',b_q)] \\
&\{K_0(\sqrt{C^{E_{26}}}|b_2'|)\theta(C^{E_{26}})+\frac{i\pi}{2}[J_0(\sqrt{C^{E_{26}}}|b_2'|)+iN_0(\sqrt{C^{E_{26}}}|b_2'|)]\theta(-C^{E_{26}})\}\int_0^1\frac{dz_1dz_2}{z_1(1-z_1)} \\
&\sqrt{\frac{X_2^{E_{26}}}{|Z_2^{E_{26}}|}}\Big\{K_1(\sqrt{X_2^{E_{26}}Z_2^{E_{26}}})\Theta(Z_2^{E_{26}})+\frac{\pi}{2}[J_1(\sqrt{X_2^{E_{26}}|Z_2^{E_{26}}|})+iN_1(\sqrt{X_2^{E_{26}}|Z_2^{E_{26}}|})]\Theta(-Z_2^{E_{26}})\Big\},
\end{aligned}
\tag{B16}
$$

where the auxiliary functions above are defined as

$$
\begin{aligned}
&A^{E_{26}}=(y-1)(1-x_1')M_{\Lambda_b}^2, B^{E_{26}}=(x_1'-1)M_{\Lambda_b}^2, C^{E_{26}}=x_2'(y-1)M_{\Lambda_b}^2,\ D^{E_{26}}=x_3yM_{\Lambda_b}^2, \\
&Z_2^{E_{26}}=A^{E_{18}}(1-z_2)+\frac{z_2}{z_1(1-z_1)}[B^{E_{18}}(1-z_1)+D^{E_{18}}z_1], \\
&X_2^{E_{26}}=[(b_2'+b_q)+z_1(b_1'-b_2'-b_q)]^2+\frac{z_1(1-z_1)}{z_2}(b_1'-b_2'-b_q)^2,
\end{aligned}
$$

$$t^{E_{26}} = max(\sqrt{|A^{E_{26}}|}, \sqrt{|B^{E_{26}}|}, \sqrt{|C^{E_{26}}|}, \sqrt{|D^{E_{26}}|}, \omega, \omega', \omega_q). \tag{B17}$$

Similarly, the factorization formula for the form factor f_2 contributed by E_{26} can be written as

$$\begin{aligned}
f_2^{E_{26}} &= G_F \frac{\pi^2}{54\sqrt{3}} f_{\Lambda_b} f_p \int [dx] \int [dx'] \int dy\, [\alpha_s(t^{E_{26}})]^2 \psi_{\Lambda_b}(x) \\
&\times \Big\{ \Big[16 m_0 M_{\Lambda_b}^4 [(C_1 - C_2) V_{ub} V_{ud}^* + ((C_3 + C_9) - (C_4 + C_{10})) V_{tb} V_{td}^*] (1-y) (\phi_M^P(y) + \phi_M^T(y)) \Big] \psi_p^V(x') \\
&\quad + \Big[16 m_0 M_{\Lambda_b}^4 [(C_1 - C_2) V_{ub} V_{ud}^* + ((C_3 + C_9) - (C_4 + C_{10})) V_{tb} V_{td}^*] (1-y) (\phi_M^P(y) + \phi_M^T(y)) \Big] \psi_p^A(x') \\
&\quad + \Big[-32 M_{\Lambda_b}^4 ((C_5 + C_7) - (C_6 + C_8)) V_{tb} V_{td}^* (y-1) [M_{\Lambda_b} (x_1' - 1) \phi_M^A(y) \\
&\qquad - m_0 (x_1' - 2) (\phi_M^P(y) + \phi_M^T(y))] \Big] \psi_p^T(x') \Big\} \\
&\times \frac{1}{16\pi^2} \int b_1' db_1' \int b_2' db_2' \int b_q db_q \int d\theta_1 \int d\theta_2 \exp[-S^{E_{26}}(x, x', y, b, b', b_q)] \\
&\quad \{ K_0(\sqrt{C^{E_{26}}} |b_2'|) \theta(C^{E_{26}}) + \frac{i\pi}{2} [J_0(\sqrt{C^{E_{26}}} |b_2'|) + i N_0(\sqrt{C^{E_{26}}} |b_2'|)] \theta(-C^{E_{26}}) \} \int_0^1 \frac{dz_1 dz_2}{z_1 (1 - z_1)} \\
&\quad \sqrt{\frac{X_2^{E_{26}}}{|Z_2^{E_{26}}|}} \Big\{ K_1(\sqrt{X_2^{E_{26}} Z_2^{E_{26}}}) \Theta(Z_2^{E_{26}}) + \frac{\pi}{2} [J_1(\sqrt{X_2^{E_{26}} |Z_2^{E_{26}}|}) + i N_1(\sqrt{X_2^{E_{26}} |Z_2^{E_{26}}|})] \Theta(-Z_2^{E_{26}}) \Big\}.
\end{aligned} \tag{B18}$$

4. Factorization formulae for the Bow-tie diagrams

For the 17th diagram in Fig. 7 (labeled as B_{17}), we have:

$$\begin{aligned}
f_1^{B_{17}} &= G_F \frac{\pi^2}{216\sqrt{3}} f_{\Lambda_b} f_p \int [dx] \int [dx'] \int dy\, [\alpha_s(t^{B_{17}})]^2 \psi_{\Lambda_b}(x) \\
&\times \Big\{ \Big[-16 M_{\Lambda_b}^5 [(-(C_5 + C_7) + (C_6 + C_8)) V_{tb} V_{td}^*] (x_3' + x_1'(y-1) - y + 1) \phi_M^A(y) \Big] \psi_p^V(x') \\
&\quad + \Big[-32 m_0 M_{\Lambda_b}^4 [(-C_1 + C_2) V_{ub} V_{ud}^* + (-(C_3 + C_9) + (C_4 + C_{10})) V_{tb} V_{td}^*] (y-1) (\phi_M^P(y) + \phi_M^T(y)) \\
&\qquad - 16 M_{\Lambda_b}^5 [(-(C_5 + C_7) + (C_6 + C_8)) V_{tb} V_{td}^*] (x_3' + x_1'(y-1) - y + 1) \phi_M^A(y) \Big] \psi_p^A(x') \\
&\quad + \Big[32 M_{\Lambda_b}^5 [(-C_1 + C_2) V_{ub} V_{ud}^* + (-(C_3 + C_9) + (C_4 + C_{10})) V_{tb} V_{td}^*] x_3' \psi_M^A(y) \\
&\qquad + 32 m_0 M_{\Lambda_b}^4 [(-(C_5 + C_7) + (C_6 + C_8)) V_{tb} V_{td}^*] (y-1) (\phi_M^P(y) + \phi_M^T(y)) \Big] \psi_p^T(x') \Big\} \\
&\times \frac{1}{32\pi^2} \int b_1' db_1' \int b_3 db_3 \int b_q db_q \int d\theta_1 \int d\theta_2 \exp[-S^{B_{17}}(x, x', y, b, b', b_q)] \int_0^1 \frac{dz_1 dz_2 dz_3}{z_1 (1 - z_1) z_2 (1 - z_2)} \\
&\quad \sqrt{\frac{X_3^{B_{17}}}{|Z_3^{B_{17}}|}} \Big\{ K_1(\sqrt{X_3^{B_{17}} Z_3^{B_{17}}}) \Theta(Z_3^{B_{17}}) + \frac{\pi}{2} [J_1(\sqrt{X_3^{B_{17}} |Z_3^{B_{17}}|}) + i N_1(\sqrt{X_3^{B_{17}} |Z_3^{B_{17}}|})] \Theta(-Z_3^{B_{17}}) \Big\}.
\end{aligned} \tag{B19}$$

where the auxiliary functions in the above expression are defined as

$$
\begin{aligned}
A^{B_{17}} &= x_3'(y-1)M_{\Lambda_b}^2, B^{B_{17}} = (x_1'-1)M_{\Lambda_b}^2, C^{B_{17}} = (y-1)(1-x_1')M_{\Lambda_b}^2,\ D^{B_{17}} = x_3x_3'M_{\Lambda_b}^2 \\
X_3^{B_{17}} &= ((-b_1'+b_3)-(-b_3+b_q)z_2-(-b_1'+b_3-b_q)z_1(1-z_2))^2 \\
&\quad +\frac{z_2(1-z_2)}{z_3}((-b_3+b_q)-z_1(-b_1'+b_3-b_q))^2+\frac{z_1(1-z_1)z_2(1-z_2)}{z_2z_3}(-b_1'+b_3-b_q)^2, \\
Z_3^{B_{17}} &= A(1-z_3)+\frac{z_3}{z_2(1-z_2)}\Big[B(1-z_2)+\frac{z_2}{z_1(1-z_1)}[C(1-z_1)+Dz_1]\Big], \\
t^{B_{17}} &= max(\sqrt{|A^{B_{17}}|},\sqrt{|B^{B_{17}}|},\sqrt{|C^{B_{17}}|},\sqrt{|D^{B_{17}}|},\omega,\omega',\omega_q). \qquad \text{(B20)}
\end{aligned}
$$

Similarly, the factorization formula for the form factor f_2 contributed by fig. B_{17} can be written as:

$$
\begin{aligned}
f_2^{B_{17}} &= G_F\frac{\pi^2}{216\sqrt{3}}f_{\Lambda_b}f_p\int[dx]\int[dx']\int dy\,[\alpha_s(t^{B_{17}})]^2\psi_{\Lambda_b}(x) \\
&\times\ \Big\{\Big[-32m_0M_{\Lambda_b}^4[(-C_1+C_2)V_{ub}V_{ud}^*+(-(C_3+C_9)+(C_4+C_{10}))V_{tb}V_{td}^*](y-1)(\phi_M^P(y)+\phi_M^T(y)) \\
&\quad +16M_{\Lambda_b}^5[(-(C_5+C_7)+(C_6+C_8))V_{tb}V_{td}^*](x_3'+x_1'(y-1)-y+1)\phi_M^A(y)\Big]\psi_p^V(x') \\
&\quad +\Big[16M_{\Lambda_b}^5[(-(C_5+C_7)+(C_6+C_8))V_{tb}V_{td}^*](x_3'+x_1'(y-1)-y+1)\phi_M^A(y)\Big]\psi_p^A(x') \\
&\quad +\Big[32M_{\Lambda_b}^5[(-C_1+C_2)V_{ub}V_{ud}^*+(-(C_3+C_9)+(C_4+C_{10}))V_{tb}V_{td}^*]x_3'\psi_M^A(y) \\
&\quad -32m_0M_{\Lambda_b}^4[(-(C_5+C_7)+(C_6+C_8))V_{tb}V_{td}^*](y-1)(\phi_M^P(y)+\phi_M^T(y))\Big]\psi_p^T(x')\Big\} \\
&\times\ \frac{1}{32\pi^2}\int b_1'db_1'\int b_3db_3\int b_qdb_q\int d\theta_1\int d\theta_2\exp[-S^{B_{17}}(x,x',y,b,b',b_q)]\int_0^1\frac{dz_1dz_2dz_3}{z_1(1-z_1)z_2(1-z_2)} \\
&\sqrt{\frac{X_3^{B_{17}}}{|Z_3^{B_{17}}|}}\Big\{K_1(\sqrt{X_3^{B_{17}}Z_3^{B_{17}}})\Theta(Z_3^{B_{17}})+\frac{\pi}{2}[J_1(\sqrt{X_3^{B_{17}}|Z_3^{B_{17}}|})+iN_1(\sqrt{X_3^{B_{17}}|Z_3^{B_{17}}|})]\Theta(-Z_3^{B_{17}})\Big\}. \qquad \text{(B21)}
\end{aligned}
$$

For the 19th diagram in Fig. 7 (labeled as B_{19}), we have:

$$
\begin{aligned}
f_1^{B_{19}} &= G_F\frac{\pi^2}{27\sqrt{3}}f_{\Lambda_b}f_p\int[dx]\int[dx']\int dy\,[\alpha_s(t^{B_{19}})]^2\psi_{\Lambda_b}(x) \\
&\times\ \Big\{\Big[-16M_{\Lambda_b}^5[(-(C_5+C_7)+(C_6+C_8))V_{tb}V_{td}^*]x_2'\phi_M^A(y)\Big]\psi_p^V(x') \\
&\quad +\Big[-64m_0M_{\Lambda_b}^4[(-C_1+C_2)V_{ub}V_{ud}^*+(-(C_3+C_9)+(C_4+C_{10}))V_{tb}V_{td}^*]\phi_M^P(y) \\
&\quad -16M_{\Lambda_b}^5[(-(C_5+C_7)+(C_6+C_8))V_{tb}V_{td}^*]x_2'\phi_M^A(y)\Big]\psi_p^A(x') \\
&\quad +\Big[32M_{\Lambda_b}^5[(-C_1+C_2)V_{ub}V_{ud}^*+(-(C_3+C_9)+(C_4+C_{10}))V_{tb}V_{td}^*]x_2'\psi_M^A(y) \\
&\quad -64m_0M_{\Lambda_b}^4[(-(C_5+C_7)+(C_6+C_8))V_{tb}V_{td}^*](x_1'-2)\phi_M^P(y)\Big]\psi_p^T(x')\Big\}
\end{aligned}
$$

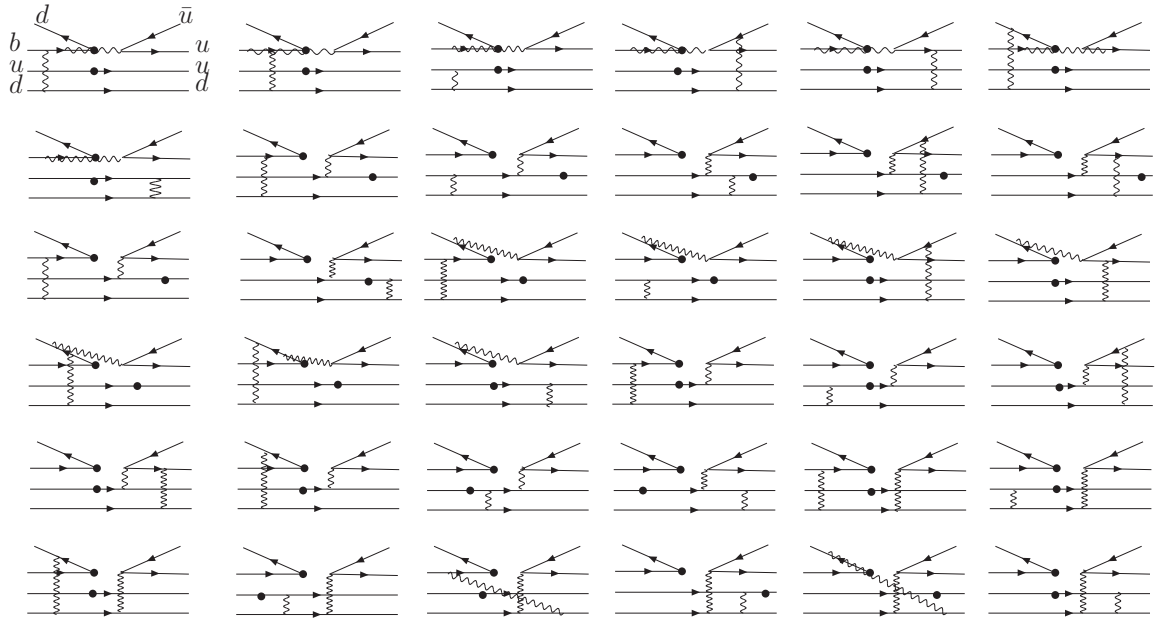

FIG. 7: Bow-tie (B) diagrams for the $\Lambda_b \to p\pi$ decay to lowest order in the pQCD approach where the dots denote the weak interactions vertices. As in the preceding figures, the two hard gluons are needed to transfer the large momentum to the light quarks in the initial state.

$$\times \frac{1}{16\pi^2}\int b_1' db_1' \int b_2' db_2' \int b_q db_q \int d\theta_1 \int d\theta_2 \exp[-S^{B_{19}}(x,x',y,b,b',b_q)]$$
$$\{K_0(\sqrt{C^{B_{19}}}|b_q|)\theta(C^{B_{19}}) + \frac{i\pi}{2}[N_0(\sqrt{C^{B_{19}}}|b_q|) + iK_0(\sqrt{C^{B_{19}}}|b_q|)]\theta(-C^{B_{19}})\}\int_0^1 \frac{dz_1 dz_2}{z_1(1-z_1)}$$
$$\sqrt{\frac{X_2^{B_{19}}}{|Z_2^{B_{19}}|}}\Big\{K_1(\sqrt{X_2^{B_{19}}Z_2^{E_{26}}})\Theta(Z_2^{B_{19}}) + \frac{\pi}{2}[J_1(\sqrt{X_2^{B_{19}}|Z_2^{B_{19}}|}) + iN_1(\sqrt{X_2^{B_{19}}|Z_2^{B_{19}}|})]\Theta(-Z_2^{B_{19}})\Big\}, \tag{B22}$$

where the auxiliary functions in the above expression are defined as:

$$A^{B_{19}} = -x_2' M_{\Lambda_b}^2, B^{B_{19}} = (x_1'-1)M_{\Lambda_b}^2, C^{B_{19}} = x_2'(y-1)M_{\Lambda_b}^2, D^{B_{19}} = x_3 x_3' M_{\Lambda_b}^2$$
$$Z_2^{B_{19}} = A^{B_{19}}(1-z_2) + \frac{z_2}{z_1(1-z_1)}[B^{B_{19}}(1-z_1) + D^{B_{19}}z_1],$$
$$X_2^{B_{19}} = [(b_2'+b_q) - z_1 b_1']^2 + \frac{z_1(1-z_1)}{z_2}{b_1'}^2$$
$$t^{B_{19}} = max(\sqrt{|A^{B_{19}}|}, \sqrt{|B^{B_{19}}|}, \sqrt{|C^{B_{19}}|}, \sqrt{|D^{B_{19}}|}, \omega, \omega', \omega_q). \tag{B23}$$

Similarly, the factorization formula for the form factor f_2 contributed by B_{19} can be written as:

$$f_2^{B_{19}} = G_F \frac{\pi^2}{27\sqrt{3}} f_{\Lambda_b} f_p \int [dx]\int [dx']\int dy\,[\alpha_s(t^{B_{19}})]^2 \psi_{\Lambda_b}(x)$$
$$\times \Big\{\Big[- 64 m_0 M_{\Lambda_b}^4 [(-C_1+C_2)V_{ub}V_{ud}^* + (-(C_3+C_9) + (C_4+C_{10}))V_{tb}V_{td}^*]\phi_M^P(y)$$

$$
\begin{aligned}
&+16M_{\Lambda_b}^5[(-(C_5+C_7)+(C_6+C_8))V_{tb}V_{td}^*]x_2'\phi_M^A(y)\Big]\psi_p^V(x')\\
&+\Big[16M_{\Lambda_b}^5[(-(C_5+C_7)+(C_6+C_8))V_{tb}V_{td}^*]x_2'\phi_M^A(y)\Big]\psi_p^A(x')\\
&+\Big[32M_{\Lambda_b}^5[(-C_1+C_2)V_{ub}V_{ud}^*+(-(C_3+C_9)+(C_4+C_{10}))V_{tb}V_{td}^*]x_2'\psi_M^A(y)\\
&+64m_0M_{\Lambda_b}^4[(-(C_5+C_7)+(C_6+C_8))V_{tb}V_{td}^*](x_1'-2)\phi_M^P(y)\Big]\psi_p^T(x')\Big\}\\
\times\ &\frac{1}{16\pi^2}\int b_1'db_1'\int b_2'db_2'\int b_qdb_q\int d\theta_1\int d\theta_2\exp[-S^{B_{19}}(x,x',y,b,b',b_q)]\\
&\{K_0(\sqrt{C^{B_{19}}}|b_q|)\theta(C^{B_{19}})+\frac{i\pi}{2}[N_0(\sqrt{C^{B_{19}}}|b_q|)+iK_0(\sqrt{C^{B_{19}}}|b_q|)]\theta(-C^{B_{19}})\}\int_0^1\frac{dz_1dz_2}{z_1(1-z_1)}\\
&\sqrt{\frac{X_2^{B_{19}}}{|Z_2^{B_{19}}|}}\Big\{K_1(\sqrt{X_2^{B_{19}}Z_2^{E_{26}}})\Theta(Z_2^{B_{19}})+\frac{\pi}{2}[J_1(\sqrt{X_2^{B_{19}}|Z_2^{B_{19}}|})+iN_1(\sqrt{X_2^{B_{19}}|Z_2^{B_{19}}|})]\Theta(-Z_2^{B_{19}})\Big\}.
\end{aligned}
\tag{B24}
$$

5. Factorization formulae for the penguin annihilation diagrams

For the 14th diagram in Fig. 8 (labeled as P_{14}), we have:

$$
\begin{aligned}
f_1^{P_{14}} \;=\;& G_F\frac{\pi^2}{54\sqrt{3}}f_{\Lambda_b}f_p\int[dx]\int[dx']\int dy\,[\alpha_s(t^{P_{14}})]^2\psi_{\Lambda_b}(x)\\
\times\ &\Big\{\Big[48M_{\Lambda_b}^4[(C_3+C_4)-\frac{1}{2}(C_9+C_{10})]V_{tb}V_{td}^*(M_{\Lambda_b}(y-1)\phi_M^A(y)+m_0(\phi_M^P(y)-\phi_M^T(y)))\\
&-32M_{\Lambda_b}^4[(C_5-\frac{1}{2}C_7)+\frac{1}{2}(C_6-\frac{1}{2}C_8)]V_{tb}V_{td}^*y(M_{\Lambda_b}x_2'\phi_M^A(y)+m_0(\phi_M^T(y)-\phi_M^P(y)))\\
&-32M_{\Lambda_b}^4[\frac{1}{2}(C_5-\frac{1}{2}C_7)+(C_6-\frac{1}{2}C_8)]V_{tb}V_{td}^*(M_{\Lambda_b}x_2'\phi_M^A(y)+m_0(y-2)\phi_M^P(y)+m_0y\phi_M^T(y))\Big]\psi_p^V(x')\\
&+\Big[48M_{\Lambda_b}^4[(C_3+C_4)-\frac{1}{2}(C_9+C_{10})]V_{tb}V_{td}^*(M_{\Lambda_b}(y-1)\phi_M^A(y)-m_0(\phi_M^P(y)-\phi_M^T(y)))\\
&+32M_{\Lambda_b}^4[(C_5-\frac{1}{2}C_7)+\frac{1}{2}(C_6-\frac{1}{2}C_8)]V_{tb}V_{td}^*y(M_{\Lambda_b}x_2'\phi_M^A(y)-m_0(\phi_M^T(y)-\phi_M^P(y)))\\
&+32M_{\Lambda_b}^4[\frac{1}{2}(C_5-\frac{1}{2}C_7)+(C_6-\frac{1}{2}C_8)]V_{tb}V_{td}^*(M_{\Lambda_b}x_2'\phi_M^A(y)-m_0(y-2)\phi_M^P(y)-m_0y\phi_M^T(y))\Big]\psi_p^A(x')\\
&+\Big[96m_0M_{\Lambda_b}^4[(C_3+C_4)-\frac{1}{2}(C_9+C_{10})]V_{tb}V_{td}^*y(\phi_M^P(y)-\phi_M^T(y))\\
&+64M_{\Lambda_b}^5y[(C_5-\frac{1}{2}C_7)+\frac{1}{2}(C_6-\frac{1}{2}C_8)]V_{tb}V_{td}^*(y-1)\phi_M^A(y)\\
&-64M_{\Lambda_b}^5[\frac{1}{2}(C_5-\frac{1}{2}C_7)+(C_6-\frac{1}{2}C_8)]V_{tb}V_{td}^*(x_3'-1)\phi_M^A(y)\Big]\psi_p^T(x')\\
\times\ &\frac{1}{16\pi^2}\int b_2db_2\int b_qdb_q\int b_2'db_2'\int d\theta_1\int d\theta_2\exp[-S^{P_{14}}(x,x',y,b,b',b_q)]\\
&\{K_0(\sqrt{C^{P_{14}}}|b_2|)\theta(C^{P_{14}})+\frac{i\pi}{2}[N_0(\sqrt{|C^{P_{14}}|}|b_2|)+iK_0(\sqrt{|C^{P_{14}}|}|b_2|)]\theta(-C^{P_{14}})\}\int_0^1\frac{dz_1dz_2}{z_1(1-z_1)}
\end{aligned}
$$

$$\sqrt{\frac{X_2^{P_{14}}}{|Z_2^{P_{14}}|}}\Big\{K_1(\sqrt{X_2^{P_{14}}Z_2^{E_{26}}})\Theta(Z_2^{P_{14}})+\frac{\pi}{2}[J_1(\sqrt{X_2^{P_{14}}|Z_2^{P_{14}}|})+iN_1(\sqrt{X_2^{P_{14}}|Z_2^{P_{14}}|})]\Theta(-Z_2^{P_{14}})\Big\}, \tag{B25}$$

where the auxiliary functions in the above expression are defined as:

$$\begin{aligned}
&A^{P_{14}}=x_2'M_{\Lambda_b}^2, B^{P_{14}}=(1-x_3'y)M_{\Lambda_b}^2, C^{P_{14}}=x_2x_2'M_{\Lambda_b}^2,\ D^{P_{14}}=x_1'(y-1)M_{\Lambda_b}^2\\
&Z_2^{P_{14}}=A^{P_{14}}(1-z_2)+\frac{z_2}{z_1(1-z_1)}[B^{P_{14}}(1-z_1)+D^{P_{14}}z_1],\\
&X_2^{P_{14}}=[(b_2+b_2')-z_1b_q]^2+\frac{z_1(1-z_1)}{z_2}{b_q}^2,\\
&t^{P_{14}}=max(\sqrt{|A^{P_{14}}|},\sqrt{|B^{P_{14}}|},\sqrt{|C^{P_{14}}|},\sqrt{|D^{P_{14}}|},\omega,\omega',\omega_q).
\end{aligned} \tag{B26}$$

Similarly, the factorization formula for the form factor f_2 contributed by P_{14} can be written as:

$$\begin{aligned}
f_2^{P_{14}} &= G_F\frac{\pi^2}{54\sqrt{3}}f_{\Lambda_b}f_p\int[dx]\int[dx']\int dy\,[\alpha_s(t^{P_{14}})]^2\psi_{\Lambda_b}(x)\\
&\times\Big\{\Big[48M_{\Lambda_b}^4[(C_3+C_4)-\frac{1}{2}(C_9+C_{10})]V_{tb}V_{td}^*(M_{\Lambda_b}(y-1)\phi_M^A(y)+m_0(\phi_M^P(y)-\phi_M^T(y)))\\
&\quad+32M_{\Lambda_b}^4[(C_5-\frac{1}{2}C_7)+\frac{1}{2}(C_6-\frac{1}{2}C_8)]V_{tb}V_{td}^*y(M_{\Lambda_b}x_2'\phi_M^A(y)+m_0(\phi_M^T(y)-\phi_M^P(y)))\\
&\quad-32M_{\Lambda_b}^4[\frac{1}{2}(C_5-\frac{1}{2}C_7)+(C_6-\frac{1}{2}C_8)]V_{tb}V_{td}^*(M_{\Lambda_b}x_2'\phi_M^A(y)+m_0(y-2)\phi_M^P(y)+m_0y\phi_M^T(y))\Big]\psi_p^V(x')\\
&\quad+\Big[48M_{\Lambda_b}^4[(C_3+C_4)-\frac{1}{2}(C_9+C_{10})]V_{tb}V_{td}^*(M_{\Lambda_b}(y-1)\phi_M^A(y)-m_0(\phi_M^P(y)-\phi_M^T(y)))\\
&\quad-32M_{\Lambda_b}^4[(C_5-\frac{1}{2}C_7)+\frac{1}{2}(C_6-\frac{1}{2}C_8)]V_{tb}V_{td}^*y(M_{\Lambda_b}x_2'\phi_M^A(y)-m_0(\phi_M^T(y)-\phi_M^P(y)))\\
&\quad+32M_{\Lambda_b}^4[\frac{1}{2}(C_5-\frac{1}{2}C_7)+(C_6-\frac{1}{2}C_8)]V_{tb}V_{td}^*(M_{\Lambda_b}x_2'\phi_M^A(y)-m_0(y-2)\phi_M^P(y)-m_0y\phi_M^T(y))\Big]\psi_p^A(x')\\
&\quad+\Big[96m_0M_{\Lambda_b}^4[(C_3+C_4)-\frac{1}{2}(C_9+C_{10})]V_{tb}V_{td}^*y(\phi_M^P(y)-\phi_M^T(y))\\
&\quad+64M_{\Lambda_b}^5y[(C_5-\frac{1}{2}C_7)+\frac{1}{2}(C_6-\frac{1}{2}C_8)]V_{tb}V_{td}^*(y-1)\phi_M^A(y)\\
&\quad+64M_{\Lambda_b}^5[\frac{1}{2}(C_5-\frac{1}{2}C_7)+(C_6-\frac{1}{2}C_8)]V_{tb}V_{td}^*(x_3'-1)\phi_M^A(y)\Big]\psi_p^T(x')\\
&\times\frac{1}{16\pi^2}\int b_2db_2\int b_qdb_q\int b_2'db_2'\int d\theta_1\int d\theta_2\exp[-S^{P_{14}}(x,x',y,b,b',b_q)]\\
&\{K_0(\sqrt{C^{P_{14}}}|b_2|)\theta(C^{P_{14}})+\frac{i\pi}{2}[N_0(\sqrt{|C^{P_{14}}|}|b_2|)+iK_0(\sqrt{|C^{P_{14}}|}|b_2|)]\theta(-C^{P_{14}})\}\int_0^1\frac{dz_1dz_2}{z_1(1-z_1)}\\
&\sqrt{\frac{X_2^{P_{14}}}{|Z_2^{P_{14}}|}}\Big\{K_1(\sqrt{X_2^{P_{14}}Z_2^{E_{26}}})\Theta(Z_2^{P_{14}})+\frac{\pi}{2}[J_1(\sqrt{X_2^{P_{14}}|Z_2^{P_{14}}|})+iN_1(\sqrt{X_2^{P_{14}}|Z_2^{P_{14}}|})]\Theta(-Z_2^{P_{14}})\Big\}.
\end{aligned} \tag{B27}$$

For the 26th diagram in Fig. 8 (labeled as P_{26}), we have:

$$f_1^{P_{26}} = G_F\frac{\pi^2}{27\sqrt{3}}f_{\Lambda_b}f_p\int[dx]\int[dx']\int dy\,[\alpha_s(t^{P_{26}})]^2\psi_{\Lambda_b}(x)$$

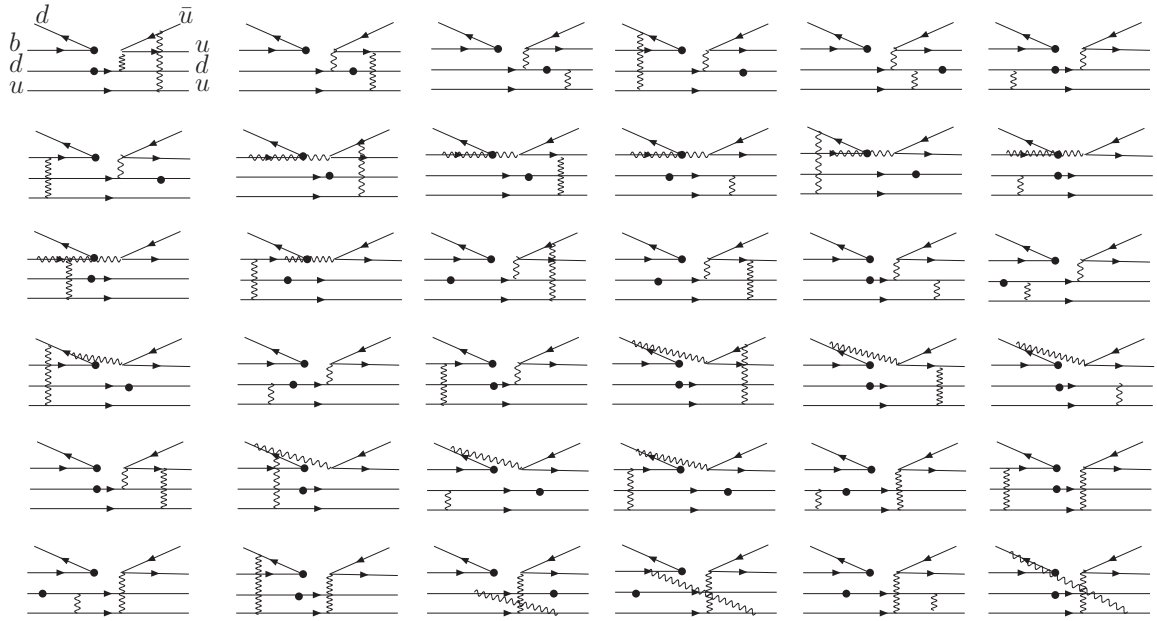

FIG. 8: Penguin annihilation (P) diagrams for the $\Lambda_b \to p\pi$ decay to lowest order in the pQCD approach where the dots denote the weak interactions vertices. As before, the two hard gluons are essential to transfer the large momentum to the light quarks in the initial state. These diagrams are called $P_1, P_2, ..., P_{36}$.

$$
\begin{aligned}
\times\ & \Big\{\Big[16M_{\Lambda_b}^4[(C_5-\frac{1}{2}C_7)-(C_6-\frac{1}{2}C_8)]V_{tb}V_{td}^*(M_{\Lambda_b}x_1'\phi_M^A(y)-2m_0(x_3'-2)\phi_M^P(y)) \\
& -16M_{\Lambda_b}^4[(C_5-\frac{1}{2}C_7)-(C_6-\frac{1}{2}C_8)]V_{tb}V_{td}^*(M_{\Lambda_b}x_1'\phi_M^A(y)+2m_0\phi_M^P(y))\Big]\psi_p^V(x') \\
& +\Big[-16M_{\Lambda_b}^4[(C_5-\frac{1}{2}C_7)-(C_6-\frac{1}{2}C_8)]V_{tb}V_{td}^*(M_{\Lambda_b}x_1'\phi_M^A(y)+2m_0(x_3'-2)\phi_M^P(y)) \\
& +16M_{\Lambda_b}^4[(C_5-\frac{1}{2}C_7)-(C_6-\frac{1}{2}C_8)]V_{tb}V_{td}^*(M_{\Lambda_b}x_1'\phi_M^A(y)-2m_0\phi_M^P(y))\Big]\psi_p^A(x')\Big\} \\
\times\ & \frac{1}{16\pi^2}\int b_1'db_1'\int b_2db_2\int b_qdb_q\int d\theta_1\int d\theta_2\exp[-S^{P_{26}}(x,x',y,b,b',b_q)] \\
& \{K_0(\sqrt{D^{P_{26}}}|b_q|)\theta(D^{P_{26}})+\frac{i\pi}{2}[N_0(\sqrt{|D^{P_{26}}|}|b_q|)+iK_0(\sqrt{|D^{P_{26}}|}|b_q|)]\theta(-D^{P_{26}})\}\int_0^1\frac{dz_1dz_2}{z_1(1-z_1)} \\
& \sqrt{\frac{X_2^{P_{26}}}{|Z_2^{P_{26}}|}}\Big\{K_1(\sqrt{X_2^{P_{26}}Z_2^{E_{26}}})\Theta(Z_2^{P_{26}})+\frac{\pi}{2}[J_1(\sqrt{X_2^{P_{26}}|Z_2^{P_{26}}|})+iN_1(\sqrt{X_2^{P_{26}}|Z_2^{P_{26}}|})]\Theta(-Z_2^{P_{26}})\Big\},
\end{aligned}
\tag{B28}
$$

where the auxiliary functions in the above expression are defined as:

$$
\begin{aligned}
& A^{P_{26}}=-x_1'M_{\Lambda_b}^2, B^{P_{26}}=(x_3'-1)M_{\Lambda_b}^2,\ C^{P_{26}}=x_2x_2'M_{\Lambda_b}^2, D^{P_{26}}=x_1'(y-1)M_{\Lambda_b}^2 \\
& Z_2^{P_{26}}=A^{P_{26}}(1-z_2)+\frac{z_2}{z_1(1-z_1)}[B^{P_{26}}(1-z_1)+C^{P_{26}}z_1], \\
& X_2^{P_{26}}=[(b_1'+b_q)-z_1b_2]^2+\frac{z_1(1-z_1)}{z_2}{b_2}^2,
\end{aligned}
$$

$$t^{P_{26}} = max(\sqrt{|A^{P_{26}}|}, \sqrt{|B^{P_{26}}|}, \sqrt{|C^{P_{26}}|}, \sqrt{|D^{P_{26}}|}, \omega, \omega', \omega_q). \tag{B29}$$

Similarly, the factorization formula for the form factor f_2 contributed by P_{26} can be written as:

$$\begin{aligned}
f_2^{P_{26}} &= G_F \frac{\pi^2}{27\sqrt{3}} f_{\Lambda_b} f_p \int [dx] \int [dx'] \int dy\, [\alpha_s(t^{P_{26}})]^2 \psi_{\Lambda_b}(x) \\
&\times \Big\{ \Big[-16 M_{\Lambda_b}^4 [(C_5 - \frac{1}{2}C_7) - (C_6 - \frac{1}{2}C_8)] V_{tb} V_{td}^* (M_{\Lambda_b} x_1' \phi_M^A(y) - 2m_0(x_3' - 2)\phi_M^P(y)) \\
&\quad -16 M_{\Lambda_b}^4 [(C_5 - \frac{1}{2}C_7) - (C_6 - \frac{1}{2}C_8)] V_{tb} V_{td}^* (M_{\Lambda_b} x_1' \phi_M^A(y) + 2m_0 \phi_M^P(y)) \Big] \psi_p^V(x') \\
&\quad + \Big[16 M_{\Lambda_b}^4 [(C_5 - \frac{1}{2}C_7) - (C_6 - \frac{1}{2}C_8)] V_{tb} V_{td}^* (M_{\Lambda_b} x_1' \phi_M^A(y) + 2m_0(x_3' - 2)\phi_M^P(y)) \\
&\quad +16 M_{\Lambda_b}^4 [(C_5 - \frac{1}{2}C_7) - (C_6 - \frac{1}{2}C_8)] V_{tb} V_{td}^* (M_{\Lambda_b} x_1' \phi_M^A(y) - 2m_0 \phi_M^P(y)) \Big] \psi_p^A(x') \Big\} \\
&\times \frac{1}{16\pi^2} \int b_1' db_1' \int b_2 db_2 \int b_q db_q \int d\theta_1 \int d\theta_2 \exp[-S^{P_{26}}(x, x', y, b, b', b_q)] \\
&\{ K_0(\sqrt{D^{P_{26}}}|b_q|)\theta(D^{P_{26}}) + \frac{i\pi}{2}[N_0(\sqrt{|D^{P_{26}}|}|b_q|) + iK_0(\sqrt{|D^{P_{26}}|}|b_q|)]\theta(-D^{P_{26}}) \} \int_0^1 \frac{dz_1 dz_2}{z_1(1-z_1)} \\
&\sqrt{\frac{X_2^{P_{26}}}{|Z_2^{P_{26}}|}} \Big\{ K_1(\sqrt{X_2^{P_{26}} Z_2^{E_{26}}})\Theta(Z_2^{P_{26}}) + \frac{\pi}{2}[J_1(\sqrt{X_2^{P_{26}}|Z_2^{P_{26}}|}) + iN_1(\sqrt{X_2^{P_{26}}|Z_2^{P_{26}}|})]\Theta(-Z_2^{P_{26}}) \Big\}.
\end{aligned} \tag{B30}$$

6. Factorization formulae for the three-gluon-vertex diagrams

Now, we can focus on the hard amplitudes contributed by the topological diagrams shown in Fig. 3 with the insertion of the three-gluon-vertex, which have been grouped in Fig. 9. It needs to be pointed out that the insertion of the three-gluon-vertex to the external and internal W emission diagrams, namely the diagrams GTi and GCi ($i = 1-4$) in Fig. 9 have null effect on the decay amplitude, since the color factors in these diagrams are proportional to $\epsilon_{ijk}\epsilon_{i'j'k'} f^{abc} (T^a)_{i'i} (T^b)_{j'j} (T^c)_{k'k}$, which equals zero taking into account the symmetry property of the structure constant f^{abc}. This is also the reason why the Feynman diagrams with the three-gluon-vertex are neglected in computing the hard amplitudes for the semi-leptonic decays of the Λ_b baryon [15, 17, 39].

For the 1st diagram in Fig. 9 (labeled as $GE1$), we have:

$$\begin{aligned}
f_1^{GE1} &= G_F \frac{\pi^2}{24\sqrt{3}} f_{\Lambda_b} f_p \int [dx] \int [dx'] \int dy\, [\alpha_s(t^{GE1})]^2 \psi_{\Lambda_b}(x) \\
&\times \Big\{ \Big[16 M_{\Lambda_b}^4 ((C_5 + C_7) - (C_6 + C_8)) V_{tb} V_{td}^* (M_{\Lambda_b}(3x_2' + x_3)\phi_M^A(y) \\
&\quad + m_0((3 - 2x_3)\phi_M^P(y) - (1 - 2y - 2x_2'))\phi_M^T(y) \Big] \psi_p^T(x') \\
&\times \frac{1}{16\pi^2} \int b_1 db_1 \int b_2' db_2' \int b_q db_q \int d\theta_1 \int d\theta_2 \exp[-S^{GE1}(x, x', y, b, b', b_q)]
\end{aligned}$$

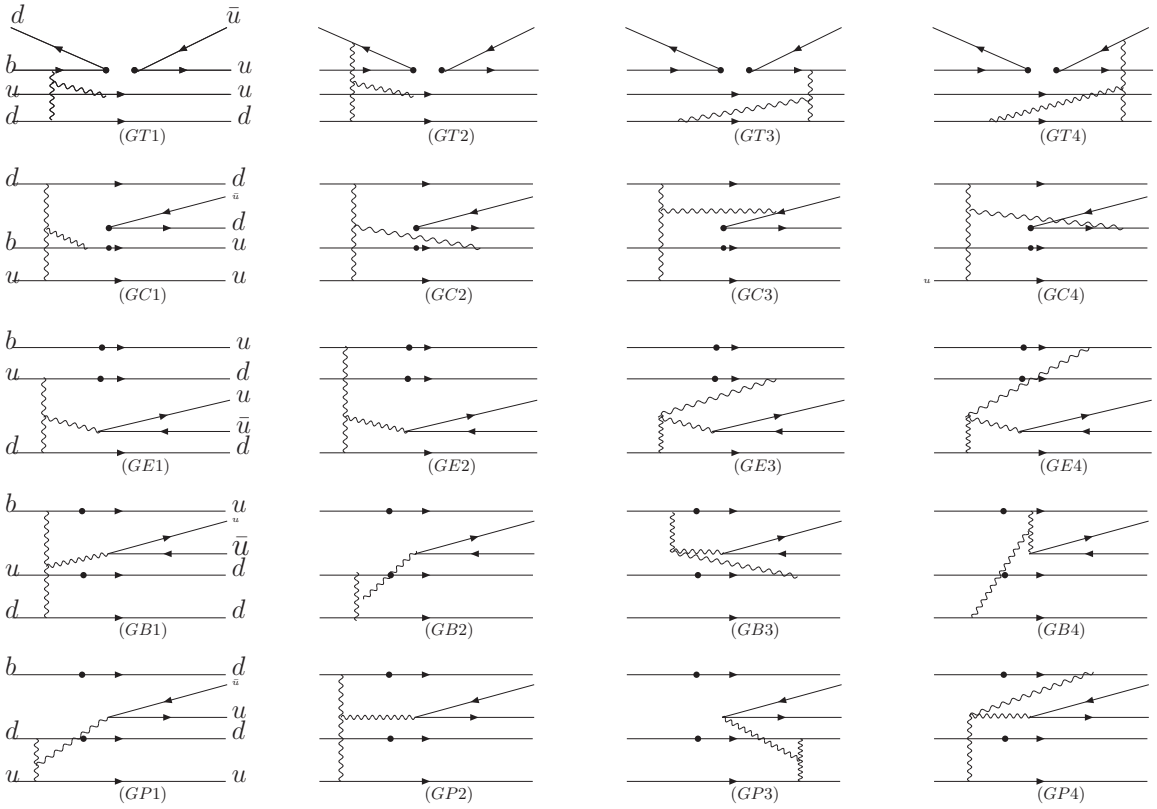

FIG. 9: Feynman diagrams responsible for the $\Lambda_b \to p\pi$ decay with three-gluon-vertex to the lowest order in the pQCD approach where the dots denote the weak interactions vertices.

$$\{K_0(\sqrt{A^{GE1}}|b_1|)\theta(A^{GE1}) + \frac{\pi i}{2}[J_0(\sqrt{|A^{GE1}||b_1|}) + iN_0(\sqrt{|A^{GE1}||b_1|})]\theta(-A^{GE1})\} \int_0^1 \frac{dz_1 dz_2}{z_1(1-z_1)}$$
$$\sqrt{\frac{X_2^{GE1}}{|Z_2^{GE1}|}}\Big\{K_1(\sqrt{X_2^{GE1}Z_2^{GE1}})\Theta(Z_2^{GE1}) + \frac{\pi}{2}[J_1(\sqrt{X_2^{GE1}|Z_2^{GE1}|}) + iN_1(\sqrt{X_2^{GE1}|Z_2^{GE1}|})]\Theta(-Z_2^{GE1})\Big\}, \tag{B31}$$

where the auxiliary functions in the expression above are defined as

$$\begin{aligned}
&A^{GE1} = -x_2' M_{\Lambda_b}^2, B^{GE1} = -x_2' M_{\Lambda_b}^2, C^{GE1} = x_2'(y-1)M_{\Lambda_b}^2,\ D^{GE1} = x_3 y M_{\Lambda_b}^2,\\
&Z_2^{GE1} = B^{GE1}(1-z_2) + \frac{z_2}{z_1(1-z_1)}[C^{GE1}(1-z_1) + D^{GE1}z_1],\\
&X_2^{GE1} = [(-b_1 + b_2' + b_q) - z_1 b_q]^2 + \frac{z_1(1-z_1)}{z_2} b_q^2,\\
&t^{GE1} = max(\sqrt{|A^{GE1}|}, \sqrt{|B^{GE1}|}, \sqrt{|C^{GE1}|}, \sqrt{|D^{GE1}|}, \omega, \omega', \omega_q).
\end{aligned} \tag{B32}$$

Similarly, the factorization formula for the form factor f_2 contributed by $GE1$ are written as:

$$f_1^{GE1} = -f_2^{GE1}. \tag{B33}$$

For the 3rd diagram in Fig. 9 (labeled as $GE3$), we have:

$$
\begin{aligned}
f_1^{GE3} &= -G_F\frac{\pi^2}{24\sqrt{3}}f_{\Lambda_b}f_p\int[dx]\int[dx']\int dy\,[\alpha_s(t^{GE1})]^2\psi_{\Lambda_b}(x)\\
&\times\Big\{\Big[-8M_{\Lambda_b}^4[(C_1-C_2)V_{ub}V_{ud}^*+((C_3+C_9)-(C_4+C_{10}))V_{tb}V_{td}^*]\\
&\quad\times(2M_{\Lambda_b}x_2'\phi_M^A(y)+m_0(3\phi_M^P(y)+(1-2y)\phi_M^T(y))\\
&\quad-8M_{\Lambda_b}^4((C_5+C_7)-(C_6+C_8))V_{tb}V_{td}^*(2M_{\Lambda_b}x_2'\phi_M^A(y)+m_0(3\phi_M^P(y)+(1-2y)\phi_M^T(y))\Big]\psi_p^V(x')\\
&\quad+\Big[-8M_{\Lambda_b}^4[(C_1-C_2)V_{ub}V_{ud}^*+((C_3+C_9)-(C_4+C_{10}))V_{tb}V_{td}^*]\\
&\quad\times(2M_{\Lambda_b}x_2'\phi_M^A(y)+m_0(3\phi_M^P(y)+(1-2y)\phi_M^T(y))\\
&\quad+8M_{\Lambda_b}^4((C_5+C_7)-(C_6+C_8))V_{tb}V_{td}^*(2M_{\Lambda_b}x_2'\phi_M^A(y)+m_0(3\phi_M^P(y)+(1-2y)\phi_M^T(y))\Big]\psi_p^A(x')\Big\}\\
&\quad+\Big[16M_{\Lambda_b}^4((C_5+C_7)-(C_6+C_8))V_{tb}V_{td}^*(x_3'-1)(M_{\Lambda_b}(2y-1)\phi_M^A(y)\\
&\quad-m_0(3(y-1)\phi_M^P(y)+(1+y)\phi_M^T(y))\Big]\psi_p^T(x')\Big\}\\
&\times\frac{1}{16\pi^2}\int b_2'db_2'\int b_3db_3\int b_qdb_q\int d\theta_1\int d\theta_2\exp[-S^{GE3}(x,x',y,b,b',b_q)]\\
&\{K_0(\sqrt{A^{GE3}}|b_2'|)\theta(A^{GE3})+\frac{\pi i}{2}[J_0(\sqrt{|A^{GE3}|}|b_2'|)+iN_0(\sqrt{|A^{GE3}|}|b_2'|)]\theta(-A^{GE3})\}\int_0^1\frac{dz_1dz_2}{z_1(1-z_1)}\\
&\sqrt{\frac{X_2^{GE3}}{|Z_2^{GE3}|}}\Big\{K_1(\sqrt{X_2^{GE3}Z_2^{GE3}})\Theta(Z_2^{GE3})+\frac{\pi}{2}[J_1(\sqrt{X_2^{GE3}|Z_2^{GE3}|})+iN_1(\sqrt{X_2^{GE3}|Z_2^{GE3}|})]\Theta(-Z_2^{GE3})\Big\},
\end{aligned}
\tag{B34}
$$

where the auxiliary functions in the above expression are defined as:

$$
\begin{aligned}
&A^{GE3}=(x_3'-1)M_{\Lambda_b}^2, B^{GE3}=-x_2'M_{\Lambda_b}^2, C^{GE3}=x_2'(y-1)M_{\Lambda_b}^2, D^{GE3}=x_3yM_{\Lambda_b}^2,\\
&Z_2^{GE3}=B^{GE3}(1-z_2)+\frac{z_2}{z_1(1-z_1)}[C^{GE3}(1-z_1)+D^{GE3}z_1],\\
&X_2^{GE3}=[(b_2{}'+b_q)-z_1b_q]^2+\frac{z_1(1-z_1)}{z_2}b_q^2,\\
&t^{GE3}=max(\sqrt{|A^{GE3}|},\sqrt{|B^{GE3}|},\sqrt{|C^{GE3}|},\sqrt{|D^{GE3}|},\omega,\omega',\omega_q).
\end{aligned}
\tag{B35}
$$

Similarly, the factorization formula for the form factor f_2 contributed by $GE3$ can be written as

$$
\begin{aligned}
f_2^{GE3} &= -G_F\frac{\pi^2}{24\sqrt{3}}f_{\Lambda_b}f_p\int[dx]\int[dx']\int dy\,[\alpha_s(t^{GE3})]^2\psi_{\Lambda_b}(x)\\
&\times\Big\{\Big[-8M_{\Lambda_b}^4[(C_1-C_2)V_{ub}V_{ud}^*+((C_3+C_9)-(C_4+C_{10}))V_{tb}V_{td}^*]\\
&\quad\times(2M_{\Lambda_b}x_2'\phi_M^A(y)+m_0(3\phi_M^P(y)+(1-2y)\phi_M^T(y))\\
&\quad-8M_{\Lambda_b}^4((C_5+C_7)-(C_6+C_8))V_{tb}V_{td}^*(2M_{\Lambda_b}x_2'\phi_M^A(y)+m_0(3\phi_M^P(y)+(1-2y)\phi_M^T(y))\Big]\psi_p^V(x')
\end{aligned}
$$

$$
\begin{aligned}
&+\Big[-8M_{\Lambda_b}^4[(C_1-C_2)V_{ub}V_{ud}^*+((C_3+C_9)-(C_4+C_{10}))V_{tb}V_{td}^*]\\
&\quad\times(2M_{\Lambda_b}x_2'\phi_M^A(y)+m_0(3\phi_M^P(y)+(1-2y)\phi_M^T(y))\\
&\quad+8M_{\Lambda_b}^4((C_5+C_7)-(C_6+C_8))V_{tb}V_{td}^*(2M_{\Lambda_b}x_2'\phi_M^A(y)+m_0(3\phi_M^P(y)+(1-2y)\phi_M^T(y))\Big]\psi_p^A(x')\Big\}\\
&+\Big[-16M_{\Lambda_b}^4((C_5+C_7)-(C_6+C_8))V_{tb}V_{td}^*(x_3'-1)(M_{\Lambda_b}(2y-1)\phi_M^A(y)\\
&\quad-m_0(3(y-1)\phi_M^P(y)+(1+y)\phi_M^T(y))\Big]\psi_p^T(x')\Big\}\\
\times\ &\frac{1}{16\pi^2}\int b_2'db_2'\int b_3db_3\int b_qdb_q\int d\theta_1\int d\theta_2\exp[-S^{GE3}(x,x',y,b,b',b_q)]\\
&\{K_0(\sqrt{A^{GE3}}|b_2'|)\theta(A^{GE3})+\frac{\pi i}{2}[J_0(\sqrt{|A^{GE3}|}|b_2'|)+iN_0(\sqrt{|A^{GE3}|}|b_2'|)]\theta(-A^{GE3})\}\int_0^1\frac{dz_1dz_2}{z_1(1-z_1)}\\
&\sqrt{\frac{X_2^{GE3}}{|Z_2^{GE3}|}}\Big\{K_1(\sqrt{X_2^{GE3}Z_2^{GE3}})\Theta(Z_2^{GE3})+\frac{\pi}{2}[J_1(\sqrt{X_2^{GE3}|Z_2^{GE3}|})+iN_1(\sqrt{X_2^{GE3}|Z_2^{GE3}|})]\Theta(-Z_2^{GE3})\Big\}.
\end{aligned}
\tag{B36}
$$

---

[1] S. Catani and L. Trentadue, Nucl. Phys. B **327** (1989) 323.

[2] J. C. Collins and D. E. Soper, Nucl. Phys. B **193** (1981) 381 [Erratum-ibid. B **213** (1983) 545].

[3] J. C. Collins, D. E. Soper and G. Sterman, Nucl. Phys. B **250** (1985) 199.

[4] M. Beneke, eConf **C0610161**, 030 (2006) [Nucl. Phys. Proc. Suppl. **170**, 57 (2007)], [arXiv:hep-ph/0612353] and references therein.

[5] Y.Y. Keum, H. -n. Li, and A.I. Sanda, Phys. Lett. **B 504**, 6 (2001) [arXiv: hep-ph/0004004]; C.D. Lü, K. Ukai, and M.Z. Yang, Phys. Rev. **D 63**, 074009 (2001) [arXiv: hep-ph/0004213].

[6] M. Beneke, G. Buchalla, M. Neubert and C. T. Sachrajda, Phys. Rev. Lett. **83**, 1914 (1999) [hep-ph/9905312]; Nucl. Phys. B**591**, 313 (2000) [hep-ph/0006124].

[7] C. W. Bauer, S. Fleming, D. Pirjol and I. W. Stewart, Phys. Rev. D **63** (2001) 114020 [arXiv:hep-ph/0011336].

[8] C. W. Bauer, D. Pirjol and I. W. Stewart, Phys. Rev. D **65** (2002) 054022 [arXiv:hep-ph/0109045].

[9] C. W. Bauer, S. Fleming, D. Pirjol, I. Z. Rothstein and I. W. Stewart, Phys. Rev. D **66** (2002) 014017 [arXiv:hep-ph/0202088].

[10] M. Beneke and T. Feldmann, Nucl. Phys. B **685**, 249 (2004) [arXiv:hep-ph/0311335].

[11] H. -n. Li, Prog. Part. Nucl. Phys. **51** (2003) 85 [arXiv:hep-ph/0303116].

[12] H. -n. Li, Phys. Rev. D **48**, 4243 (1993).

[13] B. Kundu, H. -n. Li, J. Samuelsson and P. Jain, Eur. Phys. J. C **8**, 637 (1999) [arXiv:hep-ph/9806419].

[14] H. H. Shih, S. C. Lee and H. -n. Li, Phys. Rev. D **59**, 094014 (1999) [arXiv:hep-ph/9810515].

[15] H. H. Shih, S. C. Lee and H. -n. Li, Phys. Rev. D **61**, 114002 (2000) [arXiv:hep-ph/9906370].

[16] P. Guo, H. W. Ke, X. Q. Li, C. D. Lü and Y. M. Wang, Phys. Rev. D **75**, 054017 (2007)

[arXiv:hep-ph/0501058].

[17] X. G. He, T. Li, X. Q. Li and Y. M. Wang, Phys. Rev. D **74**, 034026 (2006) [arXiv:hep-ph/0606025].

[18] C. H. Chou, H. H. Shih, S. C. Lee and H. -n. Li, Phys. Rev. D **65**, 074030 (2002) [arXiv:hep-ph/0112145].

[19] R. Mohanta, A. K. Giri and M. P. Khanna, Phys. Rev. D **63**, 074001 (2001) [arXiv:hep-ph/0006109].

[20] R. Mohanta, Eur. Phys. J. C **16** (2000) 289.

[21] V. Braun, R. J. Fries, N. Mahnke and E. Stein, Nucl. Phys. B **589** (2000) 381 [Erratum-ibid. B **607** (2001) 433] [arXiv:hep-ph/0007279].

[22] H. Y. Cheng and B. Tseng, Phys. Rev. D **48**, 4188 (1993) [arXiv:hep-ph/9304286].

[23] M. Q. Huang and D. W. Wang, Phys. Rev. D **69**, 094003 (2004) [arXiv:hep-ph/0401094].

[24] M. J. Morello [CDF Collaboration], arXiv:0810.3258 [hep-ex]; T. Altonen et al. [CDF Collaboration], arXiv:0812.4271 [hep-ex].

[25] For a review, see G. Buchalla, A. J. Buras, M. E. Lautenbacher, Rev. Mod. Phys. **68**, 1125 (1996) [hep-ph/9512380].

[26] A. Ali, G. Kramer, and C. D. Lü, Phys. Rev. D**58**, 094009 (1998) [hep-ph/9804363]; Phys. Rev. D**59**, 014005 (1998) [hep-ph/9805403]; Y. H. Chen, H. Y. Cheng, B. Tseng, and K. C. Yang, Phys. Rev. D**60**, 094014 (1999) [hep-ph/9903453].

[27] V. L. Chernyak and A.R. Zhitnitsky, Phys. Rept. **112**, 173 (1984); V. M. Braun and I. E. Filyanov, Z. Physik C**44**, 157 (1989); P. Ball, JHEP **9809**, 005 (1998) [hep-ph/9802394]; V. M. Braun and I. E. Filyanov, Z. Physik C**48**, 239 (1990); A. R. Zhitnitsky, I. R. Zhitnitsky and V. L. Chernyak, Sov. J. Nucl. Phys. **41**, 284(1985), Yad. Fiz. **41**, 445 (1985); P. Ball, JHEP **9901**, 010 (1999) [hep-ph/9812375].

[28] H. -n. Li, S. Mishima and A. I. Sanda, Phys. Rev. D **72**, 114005 (2005) [arXiv:hep-ph/0508041].

[29] F. Hussain, J. G. Körner, M. Krämer and G. Thompson, Z. Phys. C **51** (1991) 321.

[30] W. Loinaz and R. Akhoury, Phys. Rev. D **53**, 1416 (1996).

[31] C. H. Chou, H. H. Shih, S. C. Lee and H. -n. Li, Phys. Rev. D **65**, 074030 (2002).

[32] C. Amsler *et al.* [Particle Data Group], Phys. Lett. B **667**, 1 (2008).

[33] Y. M. Wang, Y. Li and C. D. Lü, Eur. Phys. J. C **59** (2009) 861 [arXiv:0804.0648].

[34] S. Groote, J. G. Körner and O. I. Yakovlev, Phys. Rev. D **56**, 3943 (1997) [arXiv:hep-ph/9705447].

[35] F. Schlumpf, arXiv:hep-ph/9211255.

[36] P. Ball, V. M. Braun and E. Gardi, Phys. Lett. B **665** (2008) 197 [arXiv:0804.2424 [hep-ph]].

[37] B. O. Lange and M. Neubert, Phys. Rev. Lett. **91**, 102001 (2003) [arXiv:hep-ph/0303082].

[38] G. P. Lepage and S. J. Brodsky, Phys. Lett. B **87**, 359 (1979).

[39] H. -n. Li, Phys. Rev. D **48**, 4243 (1993); B. Kundu, H. -n. Li, J. Samuelsson and P. Jain, Eur. Phys. J. C **8**, 637 (1999); H. H. Shih, S. C. Lee, and H. -n. Li, Phys. Rev. D **59**, 094014 (1999).

[40] V. M. Braun, A. Lenz and M. Wittmann, Phys. Rev. D **73**, 094019 (2006).

[41] J. Botts and G. Sterman, Nucl. Phys. B **325** (1989) 62.

[42] T. Kurimoto, H. -n. Li and A. I. Sanda, Phys. Rev. D **65**, 014007 (2001) [arXiv:hep-ph/0105003].

[43] H. -n. Li, Phys. Rev. D **66** (2002) 094010 [arXiv:hep-ph/0102013].

[44] Y. Y. Keum, M. Matsumori and A. I. Sanda, Phys. Rev. D **72** (2005) 014013 [arXiv:hep-ph/0406055].

[45] J. Charles et al. (The CKMfitter Group); Eur. Phys. J. C**41**, 1 (2005) [hep-ph/0406184]. The input values for the CKM parameters are taken from the unitarity fits reported for the Winter 2009 updates (http://ckmfitter.in2p3.fr/).

[46] H. -n. Li and B. Tseng, Phys. Rev. D **57**, 443 (1998) [arXiv:hep-ph/9706441].

[47] G. Bell, Nucl. Phys. B **795**, 1 (2008) [arXiv:0705.3127 [hep-ph].

[48] G. Bell, arXiv:0902.1915 [hep-ph].

[49] C. H. Chen and H. -n. Li, Phys. Rev. D **71**, 114008 (2005) [arXiv:hep-ph/0504020].

[50] H. Y. Cheng, Phys. Rev. D **56** (1997) 2799 [arXiv:hep-ph/9612223].

[51] H. Y. Cheng and B. Tseng, Phys. Rev. D **53** (1996) 1457 [Erratum-ibid. D **55** (1997) 1697] [arXiv:hep-ph/9502391].

[52] T. Mannel, W. Roberts and Z. Ryzak, Phys. Lett. B **259**, 485 (1991).